Conversion of isolated lignins to electrode and separator of electric double layer capacitor suitable for ionic liquid electrolyte

(イオン液体電解質に適した電気二重層キャパシタ用電極およびセパレータへの単離リグニンの変換)

Hokkaido University Graduate School of Agriculture
Division of Environmental Resources Doctor Course

Nutthira Pakkang

Contents

Abstract

Nowadays, electricity storage devices are very important for creating a sustainable society on the usage of renewable energy. An electric double layer capacitor (EDLC) with high power density, long cycle life, and short charging time is focused on as a complementary device to secondary batteries such as lithium-ion batteries. Taking the concept of carbon-neutral into consideration, organic parts of EDLC, *e.g.*, electrodes and separators, should be produced from renewable raw materials. Among them, lignins derived from wood are considered a promising feedstock because they are now utilized in a limited area of industry despite their vast abundance. Therefore, this study aims to produce the organic parts of EDLC from technical lignins isolated from wood on an industrial scale.

Although EDLC has a high power density, its energy density (E) is much lower than that of the secondary battery. Thereby, EDLC with high energy density is required. As E is expressed as $E \propto CV^2$, where C is a specific capacitance, and V is an applied voltage window, V strongly affects E and depends on the sorts of electrolytes. Organic electrolytes and ionic liquid (IL) electrolytes are promising because they can use under wider V of 0–3 V and 0–3.5 V, respectively, than that (0–1 V) of aqueous electrolyte. You et al. (2015b) reported EDLC with excellent power density (91 kW kg^{-1}) and energy density (42 Wh kg^{-1}) assembled with activated carbon fiber (ACF) prepared from acetic acid lignin (AL) and organic electrolyte. However, I considered the ACF was more suitable for IL electrolytes because the pore size in ACF was close to those of IL molecules rather than those of organic electrolytes. As the first attempt of this study, I assemble EDLC with the AL-based ACF and 1-ethyl-3-methylimidazolium tetrafluoroborate ($EMIBF_4$) as the IL electrolyte and evaluated the electrochemical performance, energy density in particular.

Hardwood kraft lignin (HKL) is easily obtained all over the world compared to AL. As a second attempt, HKL-based ACFs were prepared as electrode material for EDLC with high E, and a separator for the EDLC was also attempted. Finally, HKL-based EDLCs were assembled and characterized.

Preparation of ACF from AL and EDLC assembly

ACF was prepared by electrospinning of AL solution with 10 wt.% hexamethylenetetramine (HEX) in AcOH/CCl_4 (8:2 w/w) at a concentration of 35 wt.%, followed by thermostabilization, carbonization, and activation with steam (64 g). A nitrogen adsorption/desorption analysis revealed that Brunauer–Emmett–Teller (BET) specific surface areas of AL-based ACF was 1700 m^2 g^{-1}. Its average pore diameter was 0.99 nm in the micropore region. From the measurement of galvanostatic charge/discharge method (GCD), the specific capacitance of EDLC assembled with AL-based ACF, IL electrolyte, and conductive carbon black (CCB) was 124.2 F g^{-1}, and the

energy density was 53 Wh kg^{-1}, which were higher than those of EDLC with AL-based ACF and organic electrolyte. Thus, AL-based ACF was proved to be more suitable for EDLC with the IL electrolyte.

Preparation of HKL-based ACF and EDLC assembly

Polyethylene glycol (PEG) is a well-known material to improve the spinnability of lignin. In this study, PEG with a molar mass of 500 kDa was added to HKL solution at a ratio of HKL/PEG = 95/5 as a sacrificial polymer to generate a big pore in addition to an improving agent for spinning. Furthermore, 10 wt.% HEX was also added to the HKL solution in DMF/AcOH (6:4 w/w). Such HKL dope at a concentration of 35 wt.% gave fine electrospun fibers. The fibers were converted to ACF by thermostabilization, carbonization, and activation with steam (19 g). An EDLC was assembled with the resultant ACF via the same process as the assembly of AL-based EDLC. Unfortunately, the EDLC revealed a very low power density. This problem was overcome by changing the addition process of CCB; CCB suspension in acetone was sprayed during electrospinning, and the resultant EDLC exhibited energy density (45 Wh kg^{-1}) and power density (42 kW kg^{-1}).

In this study, I developed an easier assembly process of EDLC compared to the aforementioned method that prepared electrodes from fine particles of ground ACF. In the new process, EDLC was directly assembled from HKL-based ACF with an appearance of filter paper without grinding. The resultant EDLC showed a much higher energy density (91.5 Wh kg^{-1}) and power density (76.2 kW kg^{-1}) than those of EDLC assembled from ground ACF.

Preparation of HKL-based separator and EDLC assembly with HKL-based materials

Thermostabilized and electrospun fibers with the appearance of filter paper were demonstrated to be applicable as a separator of EDLC without further modification. This suitable property of the fibers for the separator was caused by the porous structure, which enabled the transportation of IL electrolyte with high viscosity. EDLC was assembled with ground HKL-based ACF, the IL electrolyte, and this separator. From GCD analysis, its electrochemical performance was shown to be 114.3 F g^{-1} of specific capacitance, 48.6 Wh kg^{-1} of energy density, and 178.4 kW kg^{-1} of power density. Thus, I successfully demonstrated EDLC assembly with HKL-based electrode and separator.

In this study, EDLC with high energy density (> 42 Wh kg^{-1}) were successfully fabricated from AL- and HKL-based electrodes and a separator. The high energy density of the EDLC was attributed to not only the IL electrolyte with a wide voltage window but also the suitable pore size of lignin-based ACFs for IL molecules. This study will contribute to the valorization of lignin and the development of EDLC from biomass, leading to the creation of a sustainable society based on renewable energy.

Abbreviations

A	Surface area of electrode
ACF-AL	Activated carbon fiber from acetic acid lignin
ACF-HKL	Activated carbon fiber from hardwood kraft lignin
ACF-HKL/PEG	Activated carbon fiber from hardwood kraft lignin and polyethylene glycol
ACF-HKL/PEG/1wt%CB	Activated carbon fiber from hardwood kraft lignin, polyethylene glycol, and 1 wt.% of carbon black
ACF-HKL/PEG/5wt%CB	Activated carbon fiber from hardwood kraft lignin, polyethylene glycol, and 5 wt.% of carbon black
ACF-HKL/PEG/CB	Activated carbon fiber from hardwood kraft lignin, polyethylene glycol, and carbon black
ACFs	Activated carbon fibers
AcOH	Acetic acid
AL	Acetic acid lignin
BET	Brunauer, Emmett, and Teller
C	Specific capacitance
CB	Carbon black
CCl_4	Carbon tetrachloride
C_{CV}	Specific capacitance from Cyclic voltammetry
CFRP	Carbon fiber reinforced plastics
CFs	Carbon fibers
C_{GCD}	Specific capacitance from Galvano static charge/ discharge
CMC	Sodium carboxymethyl cellulose
CV	Cyclic voltammetry
d	Distance between electrolyte ions and electrodes
DMF	*N*,*N*-Dimethylformamide
E	Energy density
EC	Ethylene carbonate
EDLC	Electric double layer capacitor
EDLC-AL	EDLC from acetic acid lignin
EDLC-HKL/PEG	EDLC from hardwood kraft lignin, polyethylene glycol
EDLC-HKL/PEG/1wt%CB	EDLC from hardwood kraft lignin, polyethylene glycol, and 1 wt.% of carbon black
EDLC-HKL/PEG/5wt%CB	EDLC from hardwood kraft lignin, polyethylene glycol, and 5 wt.% of carbon black

EDLC-HKL/PEG/CB	EDLC from hardwood kraft lignin, polyethylene glycol, and carbon black
EIS	Electrochemical impedance spectroscopy
$EMIBF_4$	1-ethyl-3-methylimidazolium tetrafluoroborate
G	Guaiacyl
GCD	Galvanostatic charge/discharge
H	*p*-hydroxyphenyl
HEX	Hexamethylenetetramine
Hexamine	Hexamethylenetetramine
HKL	Hardwood kraft lignin
HKL/PEG	Hardwood kraft lignin blended with polyethylene glycol
HKL/PEG/1wt%CB	Hardwood kraft lignin blended with polyethylene glycol and 1 wt.% carbon black
HKL/PEG/5wt%CB	Hardwood kraft lignin blended with polyethylene glycol and 5 wt.% carbon black
HKL/PEG/CB	Hardwood kraft lignin blended polyethylene glycol and carbon black
i	Constant current
IL	Ionic liquid
KL	Kraft lignin
LPF	Lignin-based polyester film
MA	Maleic anhydride
Na_2S	Sodium sulfide
NaOH	Sodium hydroxide
P	Power density
PAN	Polyacrylonitrile
PC	Propylene carbonate
PEG	Polyethylene glycol
PEG 500kDa	PEG with a molar mass of 500 kDa
PEG400	PEG with a molar mass of 400 Da
PEGL	Polyethylene glycol lignin
QSDFT	Quenched Solid Density Functional Theory
R_{ct}	Charge transfer resistance
R_d	Diffusion resistance
R_i	Intrinsic resistance
S	Syringyl
SAL	Softwood acetic acid lignin
T-HKL mat	Thermostabilized electrospun fiber mat of HKL

$TEMABF_4$	Triethylmethylammonium tetrafluoroborate
$TEMABF_4$/PC	Triethylmethylammonium tetrafluoroborate in propylene carbonate
TOCN	TEMPO-oxidized cellulose nanofiber
V_{drop}	Voltage drop
V_{max}	Maximum value of the voltage window
Z_{Im}	The imaginary part of impedance
Z_{Re}	The real part of impedance
ε	Dielectric constant of electrolyte

List of Tables

List of Figures

Chapter 1

General introduction and Overview

In the twentieth century, fossil resources have been used as a main source for producing electricity. However, the combustion of fossil fuels generates not only electricity but also carbon dioxide, which primarily causes the global warming (Leahy, 2021). Therefore, some developed countries are changing sources from fossil resources to renewable resources, such as solar energy, wind, hydropower, geothermal, and biomass, to produce electricity. Although solar and wind energies have been focused on among the renewable resources, they cannot give constant electricity, which depends on the climate. For a stable supply of electricity, storage devices of electricity are required.

Nowadays, secondary batteries such as lithium-ion batteries and supercapacitors are promising storage devices for electricity. However, some parts of the devices are produced from fossil resources. To reduce the usage of fossil resources, the parts should be produced from renewable materials, such as woody biomass. The aim of this study is to produce the parts of supercapacitor from plant biomass components. The detailed backgrounds to produce them are described in the following sections.

1.1. Classification of the supercapacitors and their fundamental mechanism

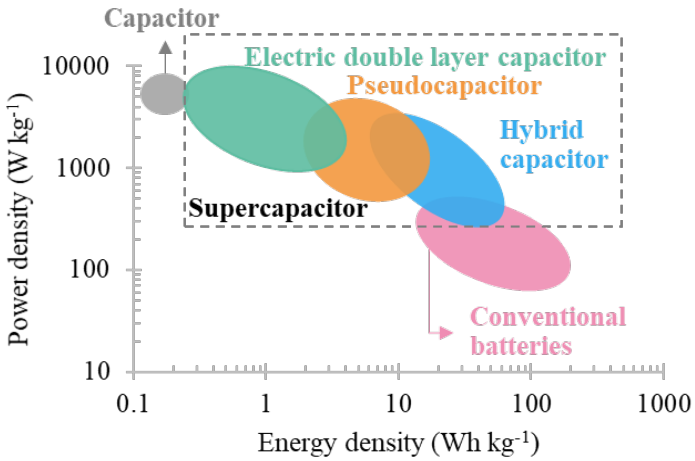

Figure 1. Ragone plot showing the specific power density against specific energy density for various electrical energy storage systems (Pohlmann, 2017).

The supercapacitor has a higher power density (rapid storage rate of energy) than the secondary batteries and can be classified into three types, electric double layer capacitor (EDLC), pseudocapacitor, and hybrid capacitor (**Figure 1**). A mechanism of storage of electricity for EDLC is caused by the physical adsorption-desorption of charged electrolytes on the electrode surface. The storage of electricity in pseudocapacitors is caused by the oxidation-reduction reaction (redox reaction) of electrolytes at a pair of electrodes, and which is called faradaic process. This process is the same as the mechanism of secondary batteries. For hybrid capacitors, the storage of electricity is caused by the combination of the faradaic process and physical adsorption-desorption. The redox reaction or faradaic process for pseudocapacitor and hybrid capacitor sometimes causes the decomposition of the electrodes or electrolytes, leading to electrochemical instability and the limitation of usage time. By contrast, EDLC exhibits excellent cycling stability and rapid charge/discharge compared to other supercapacitors. I think EDLC is a fascinating device among the supercapacitors. However, the energy density (the amount of stored energy) of EDLC is approximately 1/10 lower than those of secondary batteries (Burke 2007; Inagaki et al. 2010). Accordingly, EDLC with high energy density is required to fulfill the increasing demand for electricity, and intensive studies for the improvement have been going on.

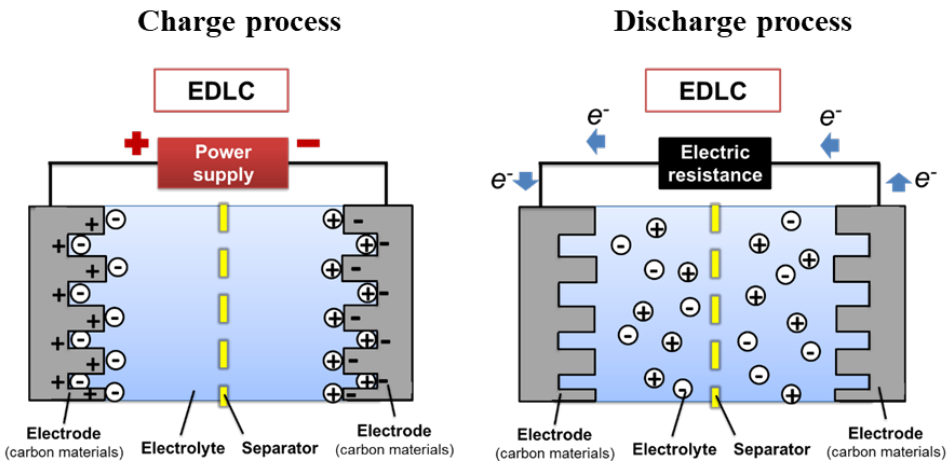

Figure 2. Mechanism of electric double layer capacitor (EDLC).

The fundamental concept of EDLC is illustrated in **Figure 2**. EDLC composes of a pair of electrodes, a separator, and an electrolyte. The electrode is the most

important part of EDLC because the specific capacitance is strongly dependent on the accessible surface area to electrolyte and surface properties, such as electrical conductivity and compatibility with electrolytes. Electrolytes are a carrier of electric charges. When EDLC is charged, cations of the electrolyte diffuse to the negative electrode, while anions of the electrolyte diffuse to the positive electrode. When fully charged, the accumulated electrolyte ions can finally form two pairs of electric layers, named the electric double layer. During discharge, electrolyte ions are gradually released from the electrode until full discharge. A separator, which is placed between two electrodes, has a main function to prevent electrical short circuits due to the direct contact of a pair of electrodes. However, it does not hamper the transportation of the charged electrolytes.

The important electrochemical performances of EDLC are energy density and power density, which are theoretically expressed as follows,

$$E = \frac{1}{8} C V^2_{max} \quad (1)$$

$$P = \frac{i\left(V_{max} - V_{drop}\right)^2}{2mV_{drop}} \quad (2)$$

E is energy density (Wh kg^{-1}), C is specific capacitance (F g^{-1}), V_{max} is the maximum value of the voltage window (V), P is power density (W kg^{-1}), i is constant current (A), and V_{drop} is the voltage drop at the beginning of the discharge (V).

An energy density (E) is proportional to the C and square of V_{max}. The width of V_{max} in EDLC is dependent on the stability of the electrolyte used. Normally, electrolytes can be divided into three types, aqueous electrolyte (aqueous KOH and aqueous H_2SO_4) (Gao et al. 2012; Daraghmeh et al. 2017), organic electrolyte (*e.g.*, triethylmethylammonium tetrafluoroborate, $TEMABF_4$) (Mhamane et al. 2013; You et al. 2015a-b), and ionic liquid (IL) electrolyte (*e.g.*, 1-ethyl-3-methylimidazolium tetrafluoroborate, $EMIBF_4$) (Hayyan et al. 2013; Mousavi et al. 2016). As shown in **Table 1**, the aqueous electrolyte has a narrow voltage window at 0-1 V because the water in the electrolyte solution is electrochemically decomposed at a higher voltage. The organic electrolyte and IL electrolyte have a wider voltage window than that of aqueous electrolytes. From equation 1, assuming that specific capacitance (C) of an electrode to any electrolytes is constant, E depends on only V_{max} of each electrolyte. When the E value

of aqueous electrolyte is normalized to 1, those of organic electrolyte and IL electrolyte are 9 and 12.3, respectively. Thus, the electrochemical stability of electrolytes significantly affects the electrochemical performance of EDLC.

Table 1. Potential window of electrolytes for EDLC

Electrolyte type	Potential window (V)	Normalized Energy density (*E*)
Aqueous (KOH)	0 - 1	1
Organic ($TEMABF_4$[a])	0 - 3	9
Ionic liquid ($EMIBF_4$[b])	0 - 3.5	12.3

[a] Triethylmethylammonium tetrafluoroborate
[b] 1-Ethyl-3-methylimidazolium tetrafluoroborate

Here I explain the factors that affect the specific capacitance (*C*) of EDLC. *C* is expressed as the following equation;

$$C = \frac{\varepsilon A}{d} \qquad (3)$$

where *A* ($m^2\ g^{-1}$) is a specific surface area of the electrode, *d* (nm) is a distance between electrolyte ions and electrodes, and ε is a dielectric constant of electrolyte.

Chmiola et al. (2006) reported the relationship between pore size of electrode and EDLC normalized capacitance. In the region I of **Figure 3**, as the mesopore size of the electrode is much bigger than the electrolyte ions, the pore slightly affects the normalized specific capacitance. By contrast, in the region III, the micropore size of the electrode remarkably affects the specific capacitance because the pore size is close to the size of electrolyte ions to give a small *d* value. Thus, many researchers focus on the development of the micropores suitable for the applied electrolyte to EDLC with high performance.

In this study, I attempted to develop the electrode for IL electrolyte from lignin to achieve EDLC with high energy density. In the next section, the history of EDLC development from lignin is explained.

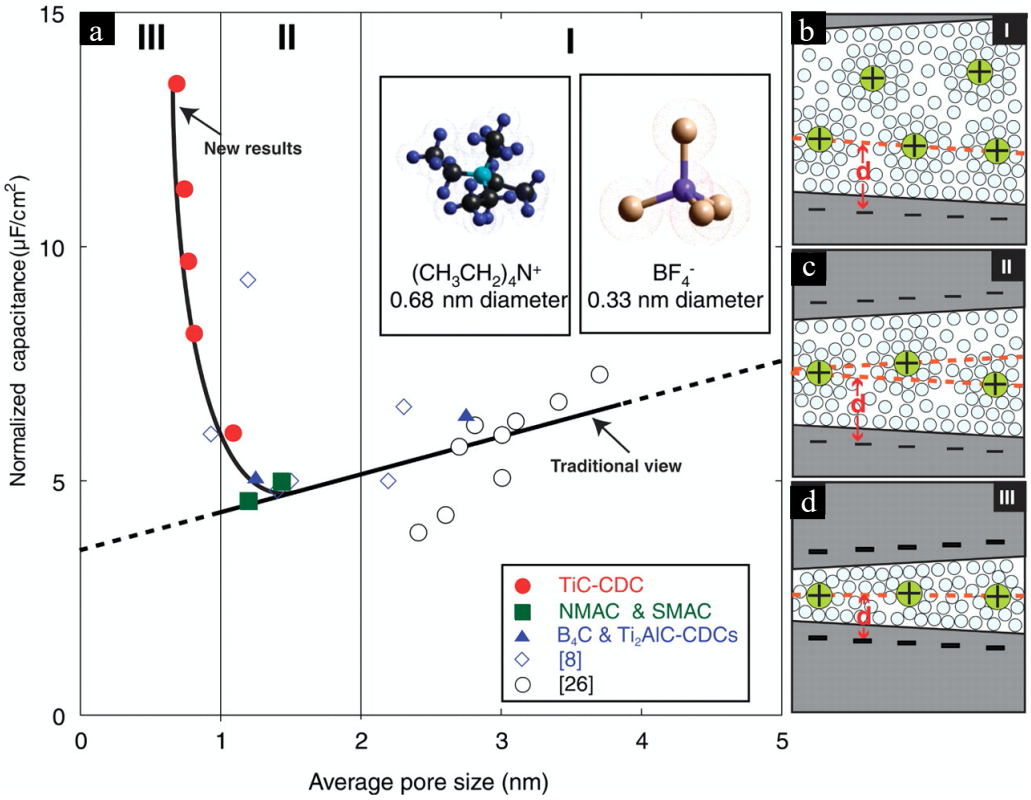

Figure 3. (a) Plot of specific capacitance and average pore size of electrode. (b to d) Drawings of electrolyte ions in pores with different distance (*d*) in pore walls; (b) greater than 2 nm, (c) between 1-2 nm, and (d) less than 1 nm.

1.2. Background for development of EDLC electrode from lignin

1.2.1. Lignin and its isolation methods

Lignin is an aromatic biopolymer and is widely found in softwoods, hardwoods, grasses, and other plants. Generally, the lignin contents are 25–35 % in softwoods, 20–25 % in hardwoods, and 15–25 % in grasses (Schutyser et al. 2018; Xu et al. 2020; Zheng et al. 2021). An important role of lignin in the plant is reported to give mechanical strength to plant cell walls by filling void space between cell walls and bonding between cellulose and hemicellulose (**Figure 4**). Another role is waterproof property. Thereby, the upward transport of water is facilitated in xylem tissues. Moreover, lignin has antimicrobial properties (Jonglertjunya et al. 2014; Alzagameem et al. 2019) and ultraviolet resistance (Sadeghifar et al. 2020), which protect the plant body from fungi, bacteria, and sunlight.

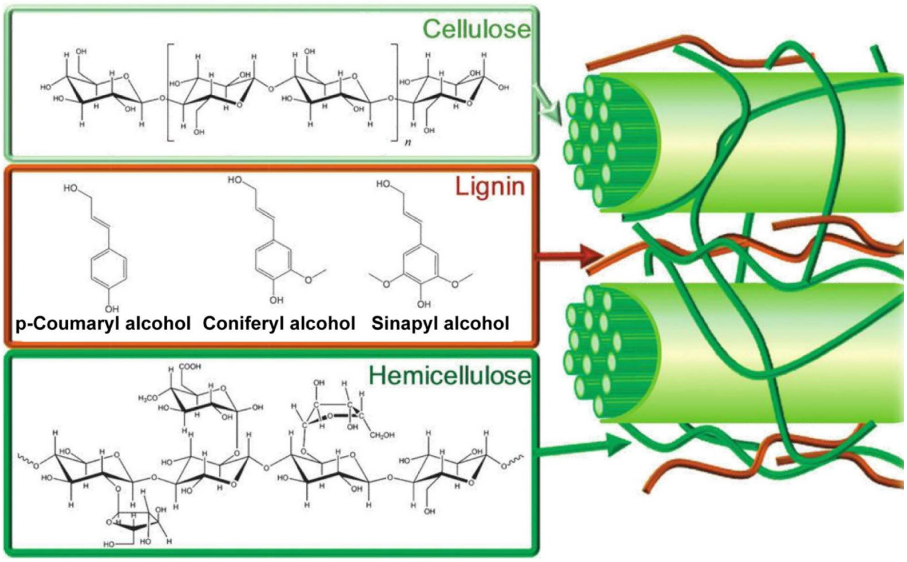

Figure 4. Typical structures of cellulose, lignin, and hemicellulose in lignocellulosic biomass (Alonso et al. 2012).

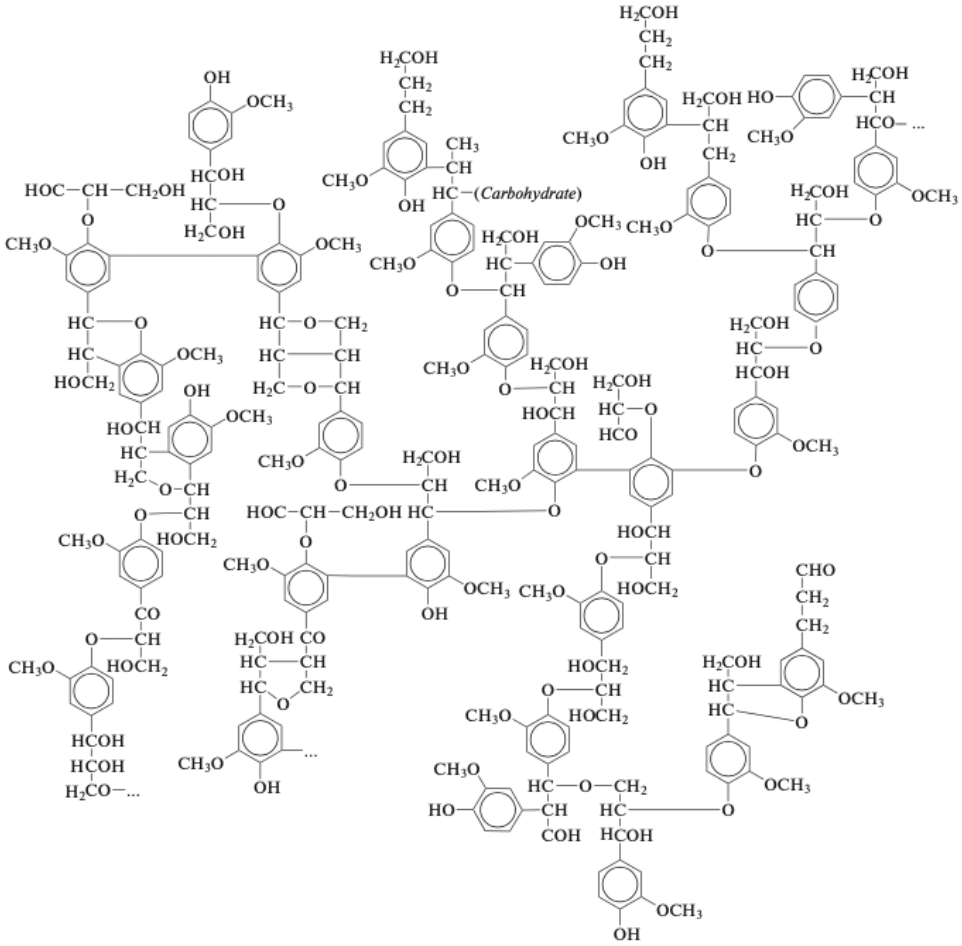

Figure 5. A proposed structure of lignin (Arapova et al. 2020).

Although a proposed structure of lignin is shown in **Figure 5**, the chemical structure and physicochemical properties of native lignin have been debated. As an example of difficulties in characterizing native lignin, an exact degree of polymerization cannot be measured because the lignin should be fragmented during the extraction process. Typical major building units called monolignols in wood are *p*-coumaryl alcohol, coniferyl alcohol, and sinapyl alcohol. The monolignol units are sometimes called *p*-hydroxyphenyl (H), guaiacyl (G), and syringyl (S) nuclei, respectively (Vanholme et al. 2010) (**Figure 6**). Softwood lignin is mainly comprised of coniferyl alcohol and a trace of *p*-coumaryl alcohol, while hardwood lignin is of sinapyl alcohol and coniferyl alcohol. The grass lignin is of H, G, and S nuclei. The main interunitary linkages of lignin are categorized as ether (C-*O*-C) linkage (β-*O*-4, α-*O*-4, 4-*O*-5) and C-C linkage (β-5, β-1, 5−5, β-β) (**Figure 7**). Among them, the β-*O*-4 bond is the most frequent interunitary linkages in the lignin substructure, accounting for more than 50% in softwoods and up to 60% in hardwoods. Therefore, the cleavage of this linkage is considered to be a key process in the chemical pulping.

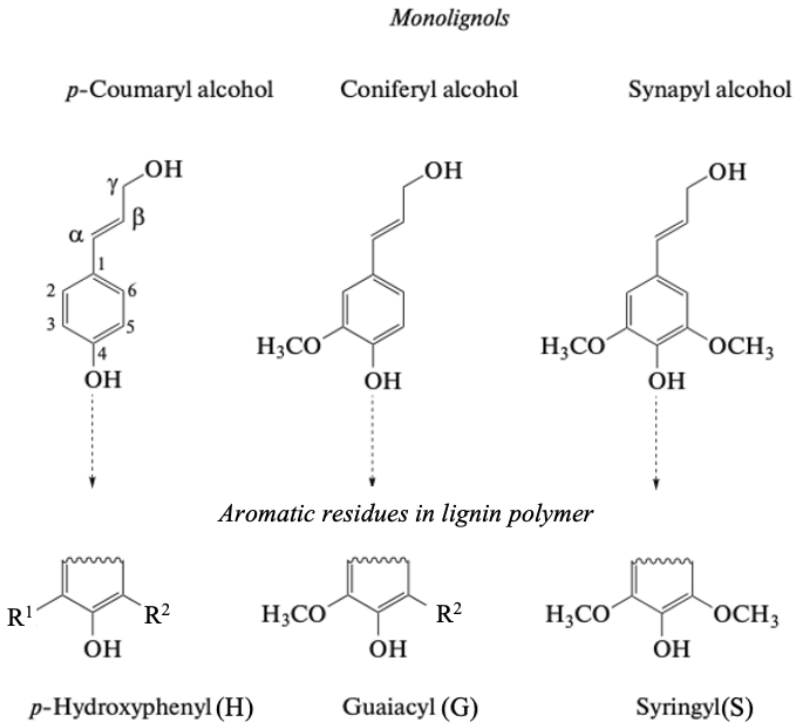

Figure 6. Major monolignols in wood and their corresponding residues in the lignin polymer.

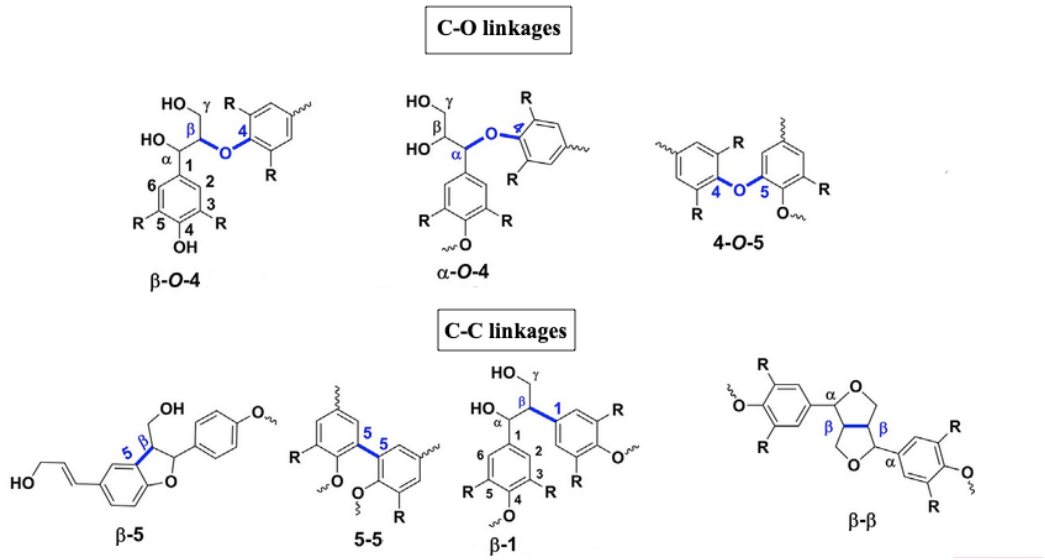

Figure 7. C-*O*-C and C-C linkages between monolignols (Dorrestijn et al. 2000).

Chemical pulping is conducted for the removal of lignin from the wood cell wall in order to get cellulose as a solid residue. There are proposed several chemical pulping methods, and a few of the methods are industrialized. The obtained lignin is called technical lignin or isolated lignin, and its chemical property depends on the isolation process. Kraft pulping is the main method (process) of chemical pulping in the world. The advantages of this process are to yield the pulp with high strength, the high recovery efficiency of used chemicals, and wide applicability for all species of hardwood and softwood. In this process, wood chips are digested at high temperatures (145–170°C) in cooking white liquor containing sodium hydroxide (NaOH) and sodium sulfide (Na_2S). During an hour of this treatment, the hydroxide and hydrosulfide anions attack the interunitary linkages of lignin. As a result, native lignin is broken into fragments, and the resultant fragments are soluble in alkaline black liquor. About 90% of lignin in black liquor can be recovered by acid precipitation and called kraft lignin (KL).

In the organosolv process, organic solvents such as methanol (Bennani et al. 1991), ethanol (Westmoreland and Jefcoat, 1991), acetic acid (Tsuchiya et al. 1991; Shukry et al. 1992), and polyethylene glycol (PEG) (Cole et al. 1993), are used as a cooking solvent with or without catalysts. The cooking is conducted at a wide range of temperatures between 77-220°C and pressures depending on the selected solvent. Organosolv lignin can be obtained by removing the cooking solvent followed by

precipitation with water. The structure of the organosolv lignins also strongly depends on the cooking solvents. For acetic acid lignin (AL), the hydroxy groups in AL are partially acetylated with acetic acid as a cooking solvent by sulfuric acid as an acid catalyst of pulping. The acetyl content is about 8% (Kubo et al. 1998). For polyethylene glycol lignin (PEGL), the polyethylene glycol (PEG) moieties are introduced into the lignin skeleton during the pulping process. The content of PEG was around 40-50% on lignin (Lin et al. 2012; Lin et al. 2013). The PEG moieties act as a soft segment in the lignin skeleton, giving PEGL an excellent thermal fusibility.

1.2.2. Conversion of technical lignin to carbonaceous materials for EDLC electrode

Technical lignins are considered as a promising precursor for carbonaceous materials, particularly carbon fibers (CFs) and activated carbon fibers (ACFs), due to their abundance and the highest carbon content among biopolymers (Mainka et al. 2015). Another attractive advantage of the technical lignins over current industrial feedstocks for CFs is inexpensive, which is estimated to be USD 1.1/kg (Fang et al. 2017), when compared to polyacrylonitrile (PAN; USD 10.2/kg) as one of the feedstocks.

Nowadays, CFs are a well-known structural material due to their high strength and lightweight. Their composite materials with plastics are practically used as carbon fiber reinforced plastics (CFRP). CFRP is widely used in the field of sports equipment, architecture, aircraft, and automotive (Dold et al. 2012; Nikoloutsopoulos et al. 2018; Daniyan et al. 2020; Singh et al. 2020).

Many papers have been reported on lignin-based CFs. In 1992, Sudo and Shimizu reported CFs from steam-exploded lignin. The tensile strength of the CFs was 0.660 GPa. Uraki et al. (1995) prepared CFs from acetic acid lignin, and the CFs showed a tensile strength of 0.035 GPa. In 2002, Kadla and co-workers prepared hardwood kraft lignin-based CFs and obtained the tensile strength at 0.422 GPa (Kadla et al. 2002). In 2012, softwood kraft lignin-based CFs were prepared. The obtained CF showed tensile strength up to 0.457 GPa (Lin et al. 2012). However, the stiffness and the tensile strength of the reported lignin-based CFs were much lower than those of commercial CFs from PAN. Therefore, an improvement of mechanical strength of lignin-based CFs is one of the urgent subjects for their practical use (Souto et al. 2018).

Uraki et al. (1997) proposed the further functionalization of lignin-based CFs with deteriorated mechanical strength. That was to convert the CFs to ACFs. ACFs can be produced by gas and chemical activations of CFs, and are a well-known porous material. Thereby, they have drawn much attention as an adsorbent for the purification of water and air. In 2001, Uraki et al. prepared ACFs with a large specific surface area of 1930 m^2/g from softwood acetic acid lignin (SAL), and they demonstrated an excellent adsorption ability, which was comparable to that of high-performance commercial ACFs.

In this century, such lignin-based ACFs are significantly focused on as an electrode material in EDLC because the ACFs will accumulate much more electrolyte in their micropores. In 2014, Hu et al. report the EDLC assembled with electrode prepared from kraft lignin-based ACFs and aqueous electrolytes (6 M aqueous KOH). Its specific capacitance reached 344 F g^{-1} with an energy density of 8.1 Wh kg^{-1} and power density of 2.98 kW kg^{-1}. You et al. (2015b) reported the EDLC assembled with the acetic acid lignin-based electrode and organic electrolytes, $TEMABF_4$, in propylene carbonate (PC). The EDLC showed a specific capacitance of 133.3 F g^{-1} with an energy density of 42 Wh kg^{-1} and power density of 91 kW kg^{-1}. Thus, organic electrolytes gave the lignin-based EDLC larger energy and power densities compared to aqueous electrolyte, and the electrochemical performance was more excellent than the lithium-ion batteries, as shown in **Figure 8**. Such lignin-based ACFs as the electrode material were prepared from electrospun fibers because electrospun fibers had very small diameters and large surface areas. When they are activated, the resultant ACFs have a remarkably large surface area and large pore volume.

Here, I show again that my first objective is to prepare EDLC with IL electrolyte to achieve much higher energy. Prior to my research (until 2017), there was no report about EDLC assembled with ACFs from electrospun lignin-based materials and IL electrolytes. However, in 2019 Jayawickramage et al. reported the EDLC assembled with ACFs prepared from kraft lignin and IL electrolyte (1-butyl-1-methylpyrrolidinium bis(trifluoromethylsulfonyl)imide) in ethylene carbonate (EC) and PC. This EDLC showed the specific capacitance at 128 F g^{-1}, energy density at 59 Wh kg^{-1}, and power density at 15 kW kg^{-1}. I finally succeeded in the preparation of EDLC with more excellent electrochemical performance from lignin-based ACFs and IL. This preparation process is

explained in detail and discussed in the later chapter. In the next section, I am going to explain the electrospinning of lignin.

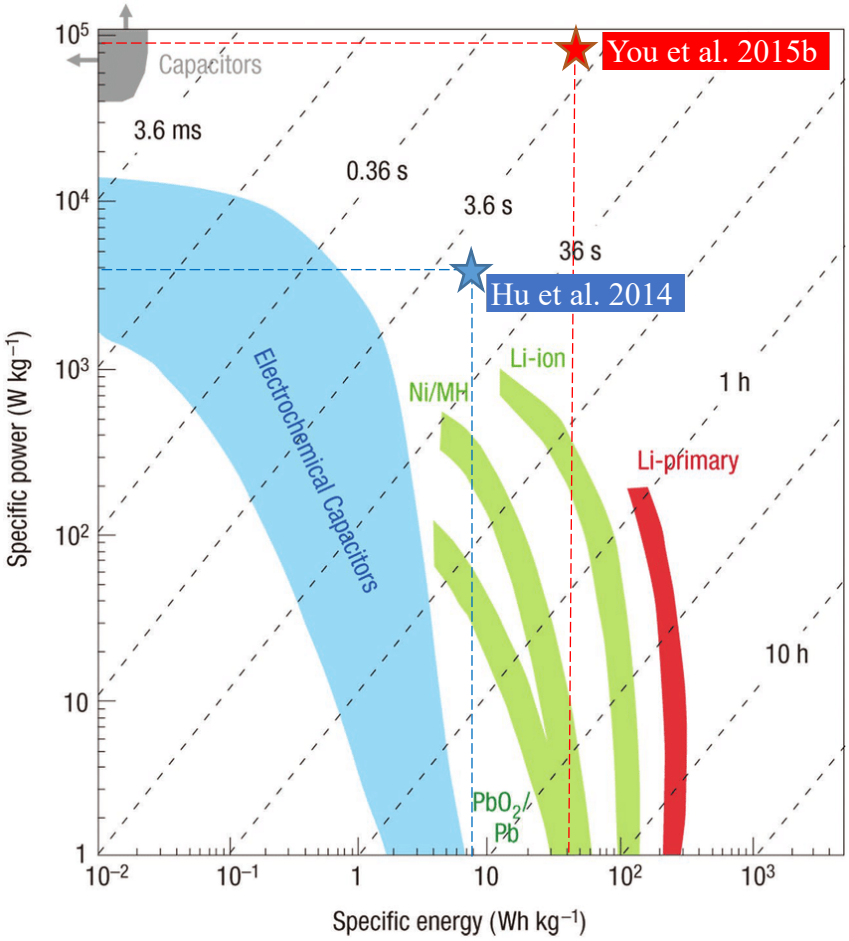

Figure 8. Ragone plot showing the reports of specific power and energy densities.

1.2.3. Electrospinning of lignin

Electrospun lignin fibers can be prepared by means of three techniques, wet-, melt-, and dry-electrospinning (**Figure 9**). Wet-electrospinning is applied to a lignin solution. The lignin solution was pushed out from the spinneret into a coagulant by the pressure. In the coagulant, lignin was solidified to form fibers. This wet-electrospinning was practically applied to the polymer blend solution of softwood kraft lignin blended and polyvinyl alcohol (Föllmer et al. 2019). When a spinneret does not contact a coagulant to make an air gap, this process is called the dry-jet wet electrospinning (Bengtsson et al. 2019).

Melt-electrospinning is applied to molten lignin. Lignin was melted by heating and extruded through a spinneret by high pressure. Then, the molten lignin was solidified at ambient temperature to form fibers. This melt-electrospinning can be applied to a PEGL (You et al. 2015a) and kraft lignin (Worarutariyachai and Chuangchote, 2020).

Dry-electrospinning is the most popular method among the electrospinning methods because it can be applied to most polymer solutions, including lignin solutions. Thereby, more detail of apparatus and mechanism are shown here. The apparatus of dry-electrospinning consists of a high voltage supplier, a spinneret with a small diameter of the needle, and a metal collector, as shown in **Figure 9-d**. A lignin solution is inserted into a syringe with a needle: the needle is connected to an electrode of the power supplier, while the metal collector is connected to the ground. By electric charging, a big electric potential is generated between the needle and the collector. Due to the electric force of the potential, the polymer is charged and formed a droplet of conical shape, named Taylor cone, at the top of the needle. When the electric force is stronger than the surface tension of the solution, a jet of the solution is emitted from the tip of the Taylor cone, and the molecules in the jet solution are stretched during flying to the collector. By this process, the jet diameter is being decreased and the solvent is also evaporated simultaneously. As a result, the solution jet transforms into fine fibers, and the fibers are deposited on the collector. So far, dry-electrospinning of acetic acid lignin (You et al. 2015b), softwood kraft lignin (Roman et al. 2019), and other types of technical lignin (Zhang et al. 2019, Kumar et al. 2019) were reported. Therefore, I also conducted this dry-electrospinning technique in this research.

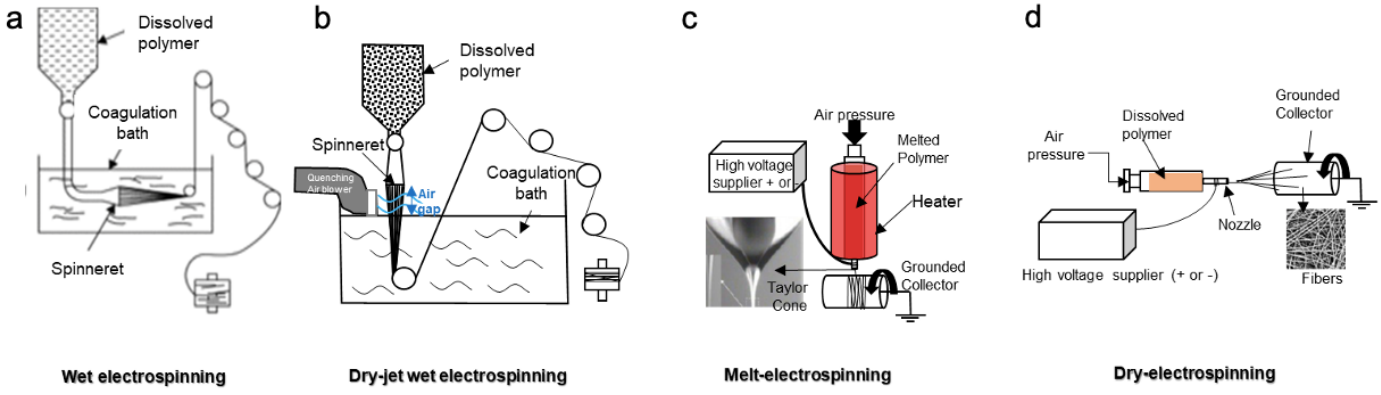

Figure 9. Fibers formation by various electrospinning methods.

1.2.4. Conversion of electrospun fibers to ACFs

The electrospun lignin fibers can be converted to ACFs by thermostabilization, carbonization, and activation. Thermostabilization is an important step to avoid fibers melting during carbonization. This step further results in increasing the strength of fibers. This step is performed by very slow heating until about 250^{o}C in an air or an oxygen atmosphere to cause the crosslinking between lignin molecules and oxygen (Braun et al. 2005; Baker and Rials, 2013). A crosslinker such as hexamethylenetetramine (Martin et al. 2006) is sometimes added to the lignin solution before electrospinning to accelerate the process. After thermostabilization, the carbonization is carried out around 1000 ^{o}C under an inert atmosphere, such as nitrogen or argon to yields lignin-based CFs (Chand, 2000). Finally, CFs can be further converted to ACFs by activation with steam (Uraki et al. 2001), carbon dioxide (Sánchez-Montero et al. 2008), and chemicals such as KOH (Huang and Zhao, 2016) and $ZnCl_2$ (Liu et al. 2016).

1.3. Development of separator part in EDLC from lignin

Besides the development of the electrode in EDLC from lignin, a separator was also developed from lignin. As far as I know, three articles on this topic were published. Koda et al. (2019) prepared a terpolyester film comprised of PEGL, maleic anhydride (MA), and polyethylene glycol with 500 kDa as a separator. Taira et al. (2019) reported TEMPO-oxidized cellulose nanofiber (TOCN)-reinforced lignin-based polyester films, which were prepared by the addition of TOCN to the above terpolyester film and demonstrated the excellent mechanical property and separator performance. Park et al. (2019) prepared a novel type of lignin hydrogel, which acts as a separator and electrolyte support. In this study, I also attempt to prepare the separator suitable for an IL electrolyte from technical lignins.

1.4. Research objective

As mentioned above, the main objectives of this research are 1) to prepare electrodes suitable for an IL electrolyte from lignin, 2) to prepare an electrode from HKL-based ACFs mat for IL electrolyte, 3) to prepare a separator suitable for an IL electrolyte from lignin.

To achieve objective 1, electrodes are prepared from acetic acid lignin (AL) and hardwood KL (HKL) *via* electrospinning, thermostabilization, carbonization, and steam activation. Afterward, EDLC is assembled with the resultant electrode, commercial separator, and commercial IL electrolyte. Although You et al. (2015b) reported the EDLC assembled with AL-based ACFs and an organic electrolyte, they did not refer to the EDLC with IL. Thereby, this research deals with two kinds of technical lignins, HKL and AL. The preparation and assembly process are explained and discussed in chapter 2.

For objective 2, electrodes are simply prepared from the mat of HKL-based ACFs. The electrode mat was directly assembled in EDLC with IL electrolyte. Their electrochemical properties are investigated and reported in chapter 3.

To achieve objective 3, two types of lignin-based separators are prepared from PEGL and KL. EDLC is assembled with the resultant separators, commercial IL electrolyte, and the electrode prepared in chapter 2. The detail of preparation and their properties are described in chapter 4. The total summary and the further subject to improve lignin-based EDLC are discussed in chapter 5 as a concluding remark.

Chapter 2

Preparation of lignin-based electrode for IL electrolyte

2.1. Introduction

In this chapter, I demonstrate the preparation of an electrode with high energy density from HKL and AL. To achieve the high energy density, the ionic liquid (IL) is a promising electrolyte because its potential window (applied voltage) is very large. To prepare an EDLC electrode suitable for IL electrolytes, the micropores with a little larger diameter than those of IL ions should be generated in an electrode material, such as activated carbon, because the distance between the wall of the micropore and the electrolyte significantly affect the specific capacitance (Chmiola et al. 2006). In this study, commercially available $EMIBF_4$ is used as an IL electrolyte (**Figure 10**), and its ion size was 0.76 nm in the longest dimension (Large et al. 2008). You et al. (2015b) reported that the average pore size of ACFs made from AL was 0.93 nm, which was larger than IL ion size. Thereby, AL-ACFs is a promising candidate as an electrode material for EDLC with IL electrolyte. As an attempt to prepare the electrode suitable for IL from HKL, HKL was blended with polyethylene glycol (PEG) as a sacrificial polymer, which is completely burned off at 400°C during carbonization under a N_2 atmosphere, as shown in **Figure 11.** After carbonization, the generation of micropores with the larger pore size will be expected.

In this chapter, the preparation of fibers from AL and HKL blended with PEG as a precursor for ACFs via electrospinning is first reported. Next, ACF preparation from the obtained fibers and its characterization are explained. Finally, electrochemical performances of EDLC assembled with the ACF and IL electrolyte are demonstrated.

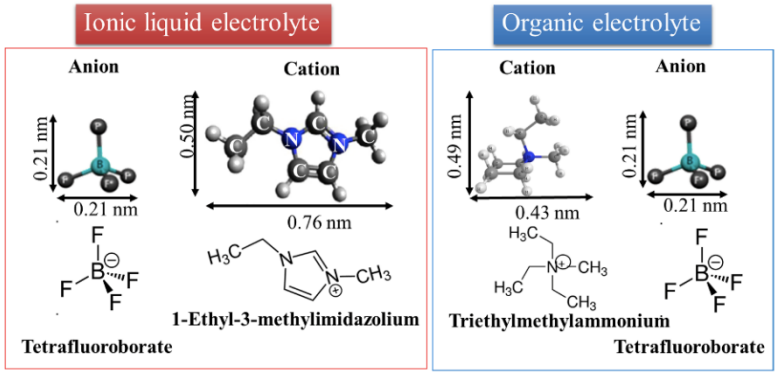

Figure 10. Anion and cation sizes in ionic liquid and organic electrolytes.

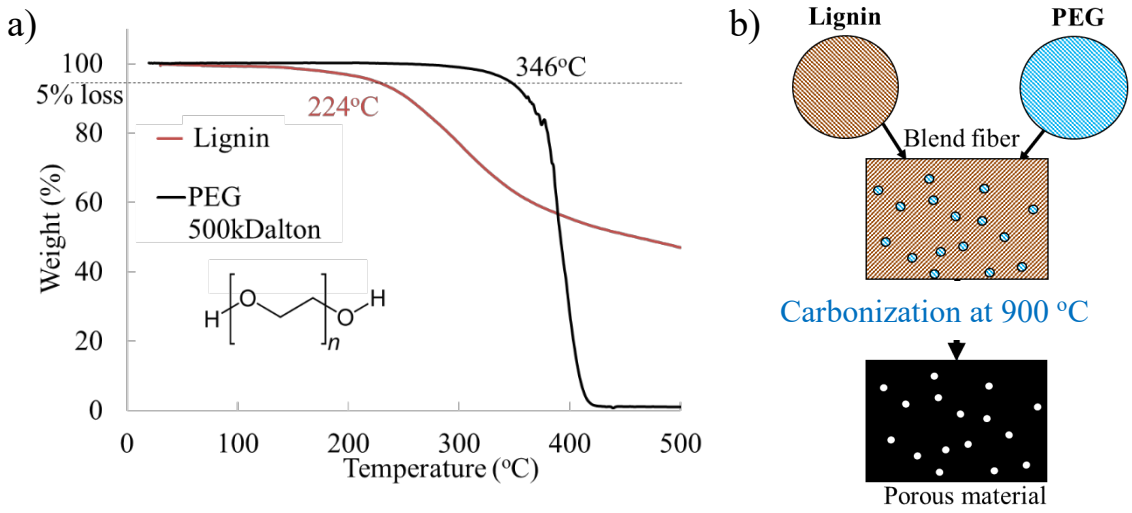

Figure 11. (a) Thermogravimetric analysis of HKL and PEG and (b) concept of micropore generation in an electrode material.

2.2. Experimental

2.2.1. Materials

AL powder was supplied by the Yingding Biotechnology Co., Ltd. (Guangzhou, China). A black liquor of hardwood kraft pulping for the preparation of hardwood kraft lignin (HKL) was provided by Nippon Paper Industries Co., Ltd. (Tokyo, Japan). Polyethylene glycol (PEG) with a molar mass of 500 kDa, acetic acid (AcOH), *N*,*N*-dimethylformamide (DMF), carbon tetrachloride (CCl_4), hexamethylenetetramine (hexamine; HEX), and sodium carboxymethyl cellulose (CMC) were purchased from FUJIFILM Wako Pure Chemical Industries, Co, Ltd. (Osaka, Japan). 1-Ethyl-3-methylimidazolium tetrafluoroborate ($EMIBF_4$) was purchased from Tokyo Chemical Industry Co, Ltd. Conductive CB was purchased from Alfa Aesar, Heysham, UK (super P conductive, 99+%). All chemicals were used as received without further purification. An aluminum sheet (0.1 mm in thickness) was purchased from Nilaco Corporation (Tokyo, Japan). Cellulosic separator (type-A sheet) was supplied by Mitsubishi Paper Mills Ltd. (Tokyo, Japan).

2.2.2. Isolation and purification of hardwood kraft lignin (HKL)

HKL was obtained from the kraft black liquor by acid precipitation with 37 wt.%. HCl at around pH 2. The precipitated lignin was filtrated with a filter paper (No.5B,

Kiriyama). The solid residue was washed with distilled water until pH reached 5 and was freeze-dried for 48-72 h to give crude HKL powder.

Twenty-five grams of crude HKL was soaked in 200 mL of 0.1 M HCI with stirring overnight. The solid was collected by vacuum filtration with a filter paper (No. 5B, Kiriyama) and washed with distilled water until the pH value became neutral. The precipitate was freeze-dried for 48 h to give purified HKL powder.

2.2.3. Purification of acetic acid lignin (AL)

AL powder (200 g) was soaked in 1000 mL of AcOH (99.7%) with stirring overnight. The solution was subjected to vacuum filtration with a filter paper (No. 5B, Kiriyama). The filtrate was concentrated by using a vacuum rotary evaporator, then poured into cold water, and the suspension was further stirred for 30 min to precipitate pure AL. The precipitated lignin was collected by vacuum filtration. The solid was washed with cold water until the pH value became neutral and freeze-dried for 48 h to give purified AL powder.

2.2.4. Electrospinning

2.2.4.1. Electrospinning of HKL

The purified HKL (1.465 g) was blended with PEG (0.077 g) at an HKL/PEG ratio of 95/5 and dissolved in a binary solvent (2.5 g) of DMF/AcOH (weight ratio; 6/4) with mixing for 1 h. Hex (0.441 g) was added to the solution and stirred further for 2 h at 80^{o}C.

An electrospinning machine was manufactured by the Machinery Laboratory in Faculty of Science, Hokkaido University (You et al. 2015a). It was composed of a power supply, a syringe with a needle as a nozzle, and a drum collector. The syringe needle with 0.8 mm of inner diameter was filled with the above lignin solution. The electrospinning was carried out under the following conditions. The applied voltage was 18 kV. The positive electrode was connected to the nozzle. Collector was connected to the ground. The distance between the nozzle and the collector was 13 cm. The extrusion rate of the solution was about 0.02 mL min^{-1}. The metallic drum collector was wrapped with a sheet of aluminum foil.

During the electrospinning of HKL/PEG solution, a 1 wt% suspension of conductive CB in acetone was repeatedly sprayed on the electrospun fiber mats until the mass of CB reached 5 wt%.

2.2.4.2. Electrospinning of AL

The purified AL was dissolved in a binary solvent of AcOH:CCl_4 (weight ratio; 8:2) at a concentration of 35 wt.% with stirring for 1 h. Ten wt.% hexamine was added to the lignin solution, and the mixture was stirred for 2 h at 80°C.

The electrospinning for the solution was carried out under the following conditions to give a mat of electrospun AL fibers: The applied voltage was 38 kV; The distance between the nozzle and the collector was 13 cm; The extrusion rate of the solution was about 0.3 mL min^{-1}.

2.2.5. Thermostabilization

Thermostabilization for the obtained mat of electrospun fibers was carried out in an electric muffle furnace (KDF S90/S90G, Denken Co. Ltd., Kyoto, Japan). The electrospun HKL fibers were heated from room temperature to 250°C at heating rates of 2°C min^{-1} under an air atmosphere, and the temperature was kept for 1 h. After cooling, thermostabilized fibers were obtained.

2.2.6. Carbonization and Activation

The carbonization and activation were successively carried out. All lignin-based-thermostabilized fibers were heated from room temperature to 900°C at a heating rate of 3°C min^{-1} under a nitrogen stream (flow rate, 0.5 L min^{-1}) in the furnace, and the temperature was kept for 1 h. After that, steam, generated by a heater, was introduced into the furnace for 1 h by a stream of N_2 gas stream for activation. After cooling, activated carbon fibers (ACFs) were obtained.

2.2.7 Electrode preparation and EDLC assembly

The ACFs prepared from AL and HKL/PEG were ground by using a pestle and a mortar and mixed homogeneously with CB. On the other hand, the ACFs prepared from HKL/PEG/CB, where CB was sprayed to deposit, were only ground without further

mixing with CB. The mixture was blended with 2% of aqueous CMC solution as a binder and homogenized by using an ultrasonic bath (5510R- DTH, Branson Ultrasonics, Emerson Japan Ltd., Tokyo, Japan) for 2 h. The weight ratio of lignin-based ACFs, CB, and CMC was 85:5:10.

Subsequently, the mixture was coated on an aluminum sheet as a current collector at an approximately 100 μm thickness by using a doctor blade, and the coated sheet was dried at 105°C overnight. Finally, the sheet was cut into a circle with 16 mm diameter and their weight was measured. The two cut sheets with almost identical weight were selected to be electrodes. The electrodes and a piece of cellulosic separator (2 cm in diameter, 33 μm in thickness) were separately immersed in IL electrolytes ($EMIBF_4$) and degassed *in vacuo* for 2 h at room temperature.

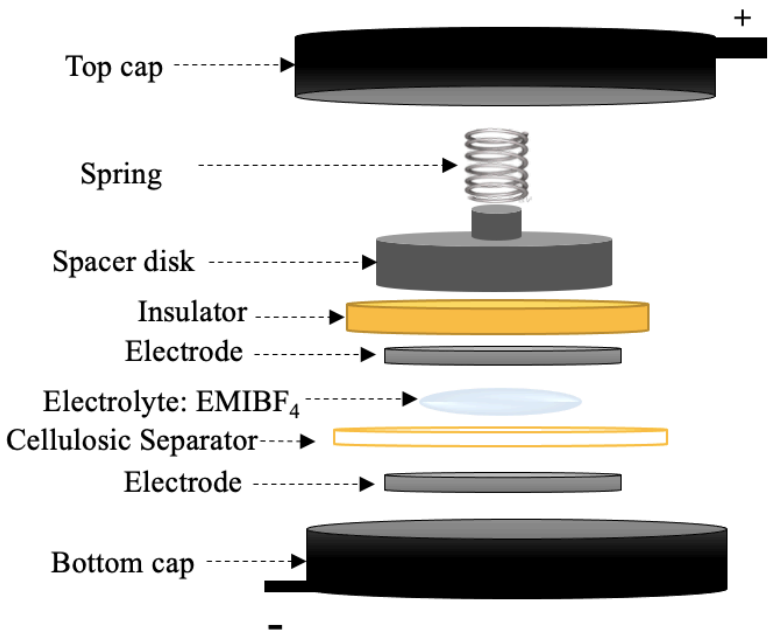

Figure 12. Structure of two electrodes cell.

Figure. 12 shows an EDLC assembly. A sheet of the prepared electrodes was placed on the bottom of the cell device (Eager Corporation, Japan), followed by a cellulosic separator and another sheet of the electrode. Finally, a spacer disk, which was connected to the analyzer, was placed on the electrode. All the processes for EDLC assembly were carried out under a N_2 atmosphere at very low humidity (RH< 5%) in a glove box.

2.2.8. Characterization

2.2.8.1. Ash content of HKL

A crucible was put into a furnace at 600°C for 1 h. It was taken out to cool down in a desiccator for 2 h. The weight of the crucible was recorded. One gram of HKL was loaded on the crucible, and which was weighed again. The crucible with lignin powder was heated at 600 °C for 12 h, then cooled down in the desiccator for 2 h. The weight of the crucible was recorded. The calculation of the percentage ash content as follows:

$$\% \text{ Ash} = \frac{(\text{wt.crucible and ash} - \text{wt.crucible})}{(\text{wt.crucible and HKL} - \text{wt.crucible})} \times 100 \quad (4)$$

2.2.8.2. Image and diameter of electrospun fibers and ACFs

Fiber morphology was observed under a 3-D laser microscope (Violet laser color 3D profile microscope VK-9500, Keyence Japan, Osaka, Japan). Fiber diameters of 20 fibers were measured at three positions for each fiber and expressed as an average diameter for 20 fibers.

2.2.8.3. Surface resistance of ACFs

The surface resistance of the ACFs was measured by using a low resistivity meter (Loresta-AX-MCP-T370, Mitsubishi Chemical Analytech, Kanagawa, Japan). A mat of ACFs was cut into 2 × 2 cm pieces. The electrical resistance was measured by pushing the probe with a linear 4-pin onto the mat surfaces at five different positions, and the average resistances were calculated.

2.2.8.4. Measurements of BET surface area and porosity

A N_2 adsorption/desorption profile of the test specimen at -196°C was monitored on a surface area analyzer (Quantachrome, Autosorb-1). Prior to the measurement, the ACFs sample was crushed and powdering and heated at 300 °C for 3 h at about 10^{-5} Pa. The specific surface area was calculated from N_2 adsorption isotherms in the range of the relative pressure ($P\ P_0^{-1}$) from 0.02 to 0.30 according to the Brunauer, Emmett, and Teller (BET) model (Fitzer and Müller, 1975). The total pore volume and average pore size were calculated from desorption isotherm, based on Quenched Solid Density Functional Theory (QSDFT) (Ravikovitch et al. 1995). In addition, a ratio of an internal and an

external surface area was estimated from the *t*-plot method in the relative pressure range of 0.2–0.5, and the internal and external surface areas were calculated based on the BET surface area and the ratio (Wang et al. 2012).

2.2.8.5. Electrochemical properties of EDLC

The performances of the prepared EDLCs were evaluated by cyclic voltammetry (CV), electrochemical impedance spectroscopy (EIS), and galvanostatic charge/discharge (GCD) method using an electrochemical workstation (Autolab PGSTAT302N FRA32M, Metrohm Autolab B.V., Tokyo, Japan).

Cyclic voltammetry (CV),

CV curves were monitored at the scan rate of 0.05 V s^{-1} within a potential window of 0-3.5 V. The specific capacitance was calculated according to the following equation (Pandit et al. 2017):

$$C_{\text{device}} = \frac{1}{mv(Vf-Vi)} \int_{Vi}^{Vf} I(V)dV \quad (5)$$

Where C_{device} is the capacitance of device (F g^{-1}), V_f and V_i, are the final and initial voltage (V), respectively, v is the scan rate (V s^{-1}), $\int_{Vi}^{Vf} I(V)dV$ is the area under the CV curve.

The equation (5) can be simplified as the following equation:

$$C_{\text{device}} = \frac{I}{m \cdot \frac{V}{t}} \quad (6)$$

Where I is the current (A) at the potential of 1.75 V (intermediate value of potential window), V/t is the scanning rate (V s^{-1}), and m (g) is the total weight of the materials on two electrodes.

Due to the two selected electrodes with almost identical weight, they are considered to be symmetric electrodes. Therefore, the specific capacitance of a single electrode (a pair of electrodes) can be calculated according to equation 7 (Qu and Shi, 1998). In this study, the calculated value is reported as specific capacitance (C_{sp}).

$$C_{sp} = 4\, C_{\text{device}} \quad (7)$$

Galvanostatic charge/discharge (GCD),

GCD measurements were carried out at a current density of 1 A g^{-1} in the voltage range of 0-3.5 V. The specific capacitance of each EDLC was calculated from the GCD curves using the formula:

$$C_{\text{device}} = \frac{i}{m \cdot \frac{dV}{dt}} \quad (8)$$

Where i is the applied current (A), $\frac{dV}{dt}$ is the slope of the discharge curve (V s^{-1}) (**Figure 13**), and m refers to the total weight (g) of the materials on two electrodes. In this study, the values of specific capacitance are C_s, which can be calculated by equation (7).

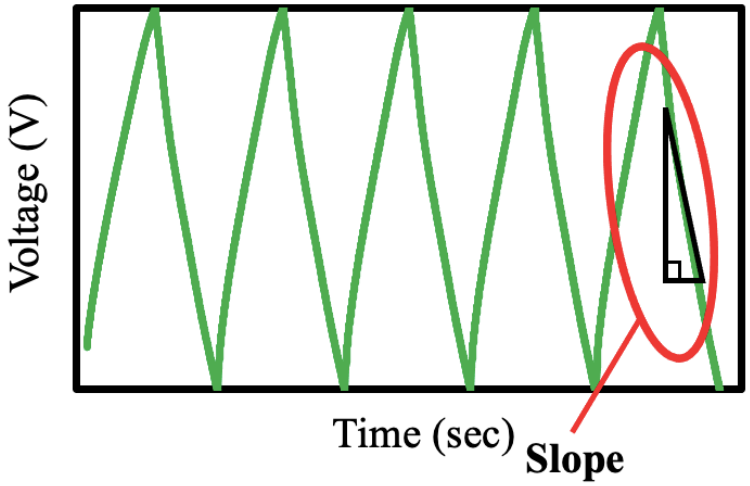

Figure 13. Galvanostatic charge/discharge (GCD) profile.

Electrochemical impedance spectroscopy (EIS),

EIS experiments were carried out at open circuit potential with a sinusoidal signal with an amplitude of 10 mV in a frequency range of 100 kHz to 1 Hz. The impedance of EDLC is caused by charge transfer, electrolyte ions diffusion, etc., which can be simulated as an equivalent circuit (named Randles equivalent circuit) in **Figure 14-a**. In the circuit, C_{dl} is a double layer capacitance, and W is Warburg impedance, which is caused by electrolyte ions diffusion.

The Nyquist plot (one of EIS) for this circuit is shown in **Figure 14-b**, and the ideal charge transfer resistance (R_{ct}) can be calculated according to the following equation:

$$(Z_{Re} - R_i - \frac{R_{ct}}{2})^2 + {Z_{Im}}^2 = \left(\frac{R_{ct}}{2}\right)^2 \quad (9)$$

where Z_{Im} and Z_{Re} are the imaginary and real parts of the complex impedance, respectively. R_i is the intrinsic resistance (Wang *et al.* 2001; Liu *et al.* 2008) and can be obtained as an interception of Z_{Re}. The R_{ct} is the chord length of the simulated impedance circle as shown in **Figure 14-b**.

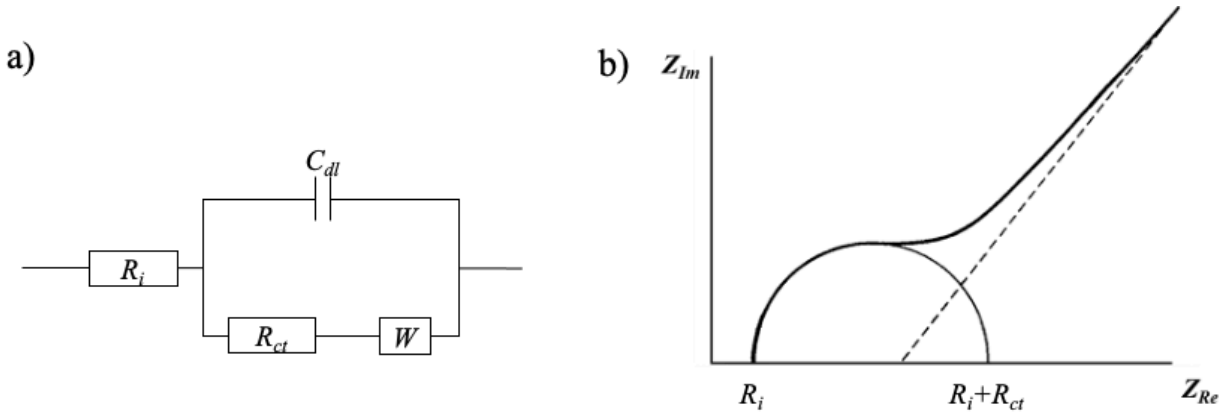

Figure 14. (a) Randles equivalent circuit (b) Nyquist plot for randles equivalent circuit.

2.3. Results and Discussion

2.3.1. Purification of hardwood kraft lignin (HKL) and acetic acid lignin (AL)

Crude HKL obtained just after the acid precipitation had a very high content (5.20%) of Ash. Since the high ash content might affect the yield and carbon content of the lignin-based ACFs, the purification was performed. When HKL was purified with 1 M of HCl aqueous solution to remove the ash, the ash content of HKL was remarkably decreased to 0.18%. In the case of AL, the ash content was significantly reduced from 0.28% to 0.16% by the purification with glacial acetic acid.

2.3.2. Electrospinning of HKL and AL

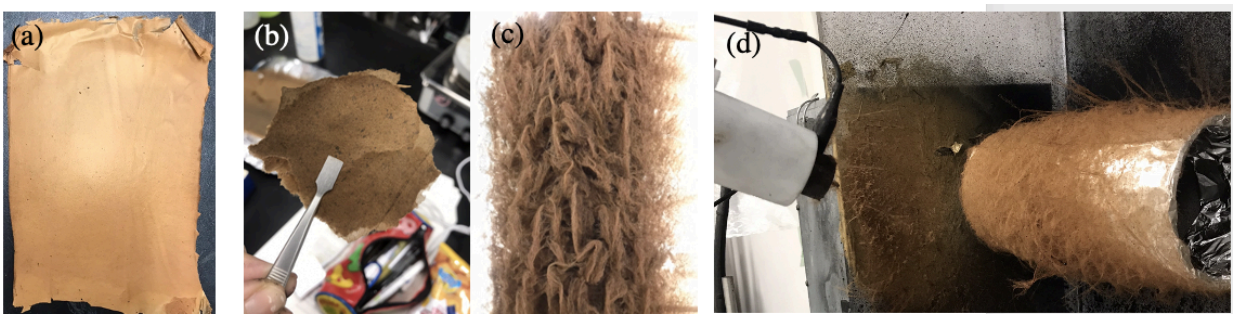

Figure 15. Photograph of electrospun fibers prepared from (a) KL/PEG (b) KL/PEG/CB (c) AL. (d) electrospinning of AL fibers

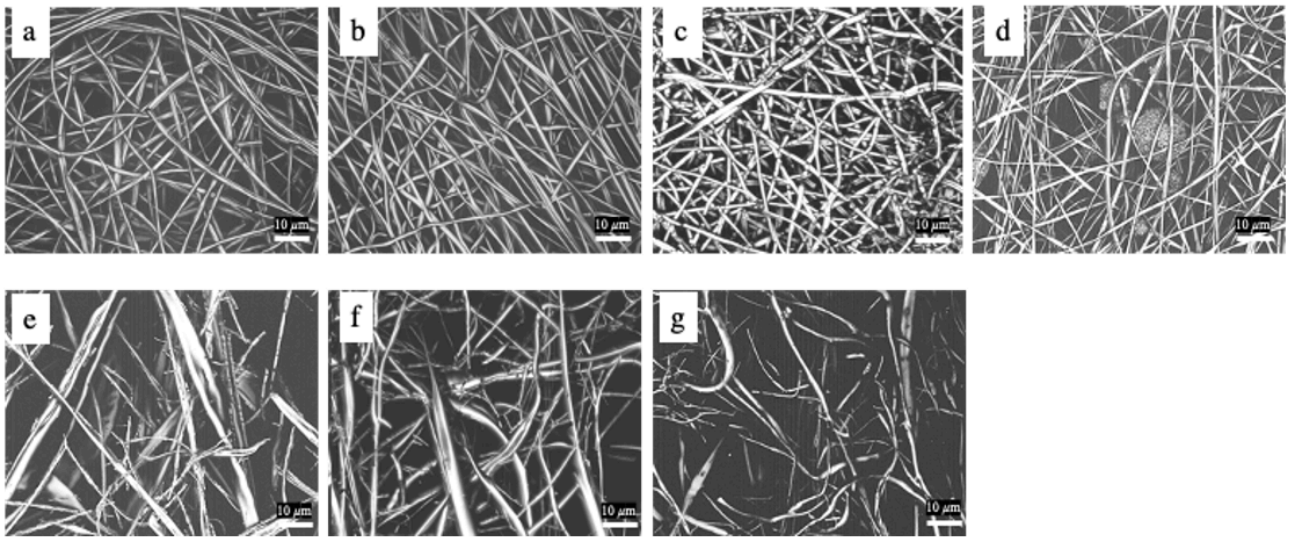

Figure 16. Microscopic images of (a - c) electrospun fibers, thermostabilized fibers, and ACFs prepared from KL/PEG, respectively, (d) ACFs prepared from KL/PEG/CB, (e - g) electrospun fibers, thermostabilized fibers, and ACFs prepared from AL, respectively.

Figure 15 showed photographs of electrospun fibers prepared from HKL/PEG, HKL/PEG/CB, and AL. Electrospinning of HKL yielded a fiber mat like a paper sheet (**Figure 15-a** and **b**), whereas that of AL gave wool-like fibers (**Figure 15-c**).

Figure 16 presented microscopic images taken by the 3-D laser microscope for HKL fibers electrospun from the dope containing 10 wt.% hexamine at 35 wt.% concentration, its thermostabilized fibers, and ACFs. Besides, the corresponding AL-based fibers were also shown for reference. The fiber diameters before and after thermostabilization are shown in **Table 2**. HKL-based fibers, HKL/PEG fibers, and

HKL/PEG/CB fibers showed a small diameter of 0.99 ± 0.21 μm and 1.08 ± 0.27 μm, respectively. By contrast, the AL-based fibers showed the thickest diameter with a larger deviation (1.71 ± 1.58 μm) compared to those of HKL/PEG fibers and HKL/PEG/CB fibers. Thus, HKL-based fibers were uniform, while AL-based fibers were non-uniform. The fiber morphology might be depended on the electrospinning conditions, especially dope solvent. The solvent for AL was AcOH/CCl_4. Since the binary solvent was evaporated faster than DMF/AcOH of the dope solvent for HKL, AL was easily solidified and stacked at the nozzle to hamper the formation of the jet. Therefore, both of higher extrusion rate and applied voltage for stable AL electrospinning were required as compared with HKL spinning conditions to prevent the solidification, as described in the Experimental part. As a result of different severity in the spinning conditions, wool-like fibers (**Figure 15-c**) and non-uniform fibers (**Figure 16-e**) were obtained.

Table 2. Average diameter of electrospun fibers before and after thermostabilization at 2 ^{o}C min^{-1} and ACFs.

Samples	Solvent	Solvent ratio	Diameter (μm)		
			Thermostabilization		Activation
			Before	After	
KL/PEG	DMF/AcOH	6/4	0.99 ± 0.21	0.83 ± 0.18	0.63 ± 0.10
KL/PEG/CB	DMF/AcOH	6/4	1.08 ± 0.27	0.97 ± 0.15	0.94 ± 0.16
AL	AcOH/CCl_4	8/2	1.71 ± 1.58	1.40 ± 0.60	1.14 ± 0.54

2.3.3. Thermostabilization of Electrospun fibers and their conversion to ACFs

The lignin fibers with 10 wt.% of hexamine were, in turn, converted to thermally stable fibers by thermostabilization by heating up to 250°C at a heating rate of 2°C min^{-1} under an air atmosphere. The complete thermostabilization was confirmed from the fact that fibers were not melted at 900 ^{o}C. In this process, hexamine is decomposed in the acidic condition to form the equivalent of formaldehyde that will act as a crosslinker, similarly to the preparation of phenol resin (Martin et al. 2006). Therefore, the addition of hexamine could increase crosslinking frequency to suppress the deformation of lignin-based fibers at elevated temperature. The thermostabilization also contributes to reducing fiber diameter as shown in **Figure 16-b, 16-f,** and **Table 2**.

The thermostabilized lignin fibers were further subjected to carbonization and steam activation processes, which were performed by heating at 900 °C for 1 h and at 900 °C for 1 h under a N_2 stream. AL-based ACFs could be obtained by the introduction of steam (64 g) into the furnace together with N_2. However, the steam activation for HKL fibers with the same amount provided only ash, but not ACFs. The applied steam was excess. Finally, the activation for the HKL-based fibers was successfully performed by applying 19 g of steam. The morphology of the resultant ACFs is depicted in **Figure 16-c, -d, and -g.**

2.3.3. Surface resistance

To characterize the obtained ACFs, the surface resistance of ACFs mat prepared from HKL/PEG and AL was first measured and found to be 3678 ± 1019 Ω and 1124 ± 298 Ω, respectively. The surface resistance of HKL/PEG-ACF was very high, resulting in a negative impact on EDLC efficiency. An addition of conductive CB was anticipated to be one of the solutions to reduce its high resistance of HKL/PEG-ACFs mat. On the other hand, AL was anticipated not to require the CB.

As a first attempt of the CB addition, CB was directly mixed with the HKL/PEG solution prior to electrospinning. Disappointedly, the electrospinning of such mixtures could not be done due to the very high viscosity of the mixture solution and the aggregation of CB particles at the nozzle of the syringe. Thereby, I attempted another method: a suspension of CB/acetone was sprayed onto electrospun fibers of HKL/PEG during the electrospinning. The resultant fibers were then converted to ACFs via thermostabilization, carbonization, and steam activation, which were named HKL/PEG/CB-ACFs. Its surface resistance was dramatically reduced to 547 ± 16 Ω by the deposition of the conductive CB.

In the next section, N_2 adsorption/desorption was measured to further characterize lignin-based ACFs with respect to surface area and pore size.

2.3.4. Determination of surface area and pore volume

The BET method was adopted to determine the specific surface area of the obtained fibers. **Figure 17** shows a hysteresis loop in the N_2 adsorption/desorption

isotherms of ACFs prepared from HKL/PEG, HKL/PEG/CB, and AL, indicating the presence of mesopores according to IUPAC physisorption isotherms (Sing, 1982).

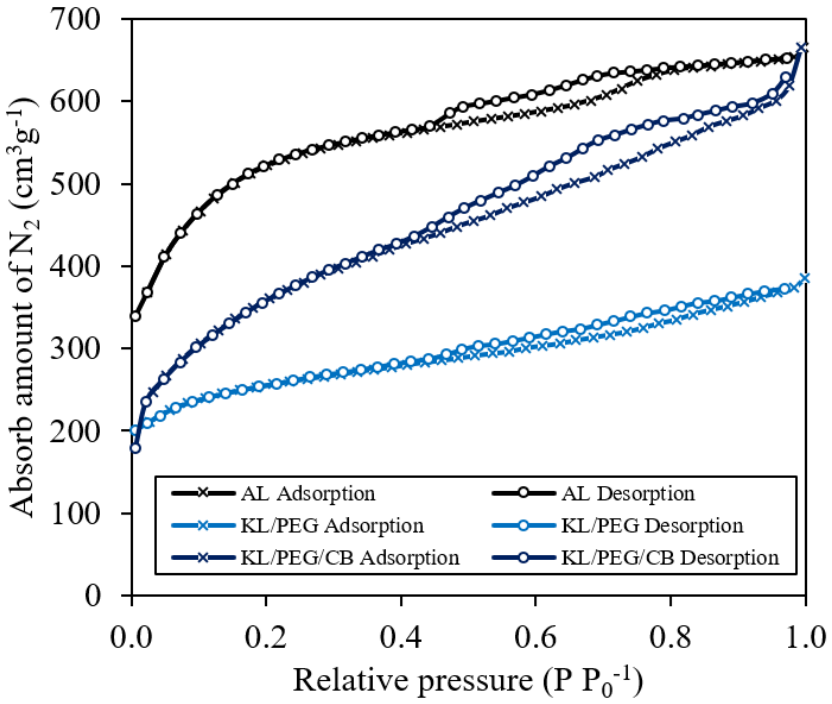

Figure 17. N_2 adsorption/desorption isotherms of the resultant ACFs.

Table 3. Textural properties of resultant activated materials.

Samples	BET surface area [a] (m^2/g)	Total pore volume [b] (ml/g)	Average pore diameter [b]				Internal surface area [c] (m^2/g)	External surface area [c] (m^2/g)
			Micropore area		Mesopore area			
			(nm)	(%)	(nm)	(%)		
HKL/PEG	816	0.48	0.84	87.4	3.16	12.7	568	248
HKL/PEG/CB	1237	0.82	1.15	73.7	3.09	26.3	565	672
AL	1700	0.92	0.99	90.4	2.95	9.6	1340	360

[a] Calculated by the BET model.
[b] Calculated based on QSDFT model.
[c] Calculated according to *t*-plot method.

Table 3 summarizes the BET specific surface area, external and internal surface areas, pore size distribution, and total pore volume calculated from the isotherms for all prepared ACFs. The internal surface area, volumes of micropore and mesopore are important parameters to represent the area of adsorption sites, while the external surface area and volume of macropores are parameters to concern the transportation of adsorbate and the area of non-adsorption sites. According to IUPAC pore size classifications,

micropores have a diameter of less than 2 nm, mesopores have a diameter of 2-50 nm, and macropores have a diameter greater than 50 nm.

The BET specific surface area of AL-based ACFs (1700 m^2 g^{-1}) was higher than those of HKL-based ACFs (HKL/PEG and HKL/PEG/CB). Moreover, the internal surface area of AL-ACF was almost 3 times larger than those of the HKL-based ACFs. This result must be related to activation efficiency; Thermostabilized AL- fibers were effectively activated with a large amount of steam without ash formation (64 mL for ACF-AL and 19 mL for ACF-HKL). Comparing ACFs from HKL/PEG and HKL/PEG/CB, ACFs from HKL/PEG/CB (1237 m^2 g^{-1}) showed higher BET specific surface area than ACFs from HKL/PEG (816 m^2 g^{-1}) even though both ACFs were activated under the same conditions. In addition, the external surface area (672 m^2 g^{-1}) of ACFs from HKL/PEG/CB was three times larger than HKL/PEG (248 m^2 g^{-1}), although both internal surface areas were almost identical. These results also reveal that CB particles must affect the activation process, especially macropore generation.

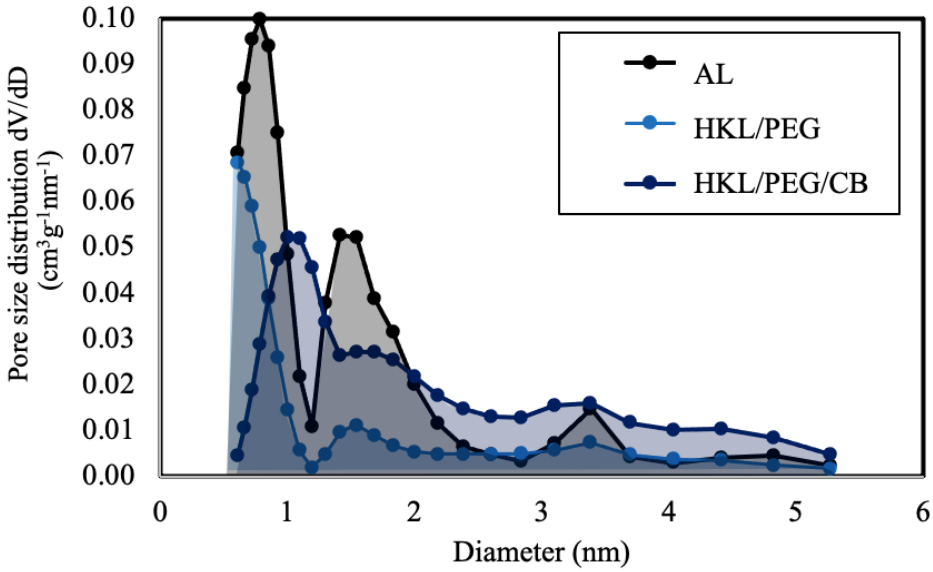

Figure 18. Pore size distribution of the resultant ACFs.

Concerning the pore diameter of ACFs in **Figure 18 and Table 3**, AL-ACFs had a pore size of 0.99 nm and had the highest micropore area (90.4%) among lignin-based ACFs. In the case of HKL-based ACFs, HKL/PEG/CB-ACFs (1.15 nm) had a larger pore size than the HKL/PEG-ACFs (0.84 nm). Both average diameters of micropore are larger than the size of IL ion (0.74 nm), indicating that expected ACFs were prepared. From the

viewpoint of mesopore, the mesopore area of ACF-HKL/PEG/CB was two times larger than that of ACF-HKL/PEG, although both average diameters were very similar. Therefore, the spraying of CB can enlarge the pore size of ACF-HKL/PEG, probably due to the CB inserted into vacant space between the fibers, resulting in expanding the space and allowing steam to penetrate into the space easily. As a result, steam activation provided ACF with a bigger pore size (**Figure 16-d**).

2.3.5. Electrochemical performance of EDLCs

EDLC was assembled with electrode prepared from ACF-HKL/PEG, ACF-HKL/PEG/CB, and ACF-AL with an ionic liquid electrolyte, $EMIBF_4$, and commercial cellulosic separator. These assembled EDLCs with a pair of electrodes prepared from electrode material of identical weight were called a two-electrode symmetrical cell. The electrochemical properties of such EDLCs were evaluated by cyclic voltammetry (CV), galvanostatic charge/discharge (GCD), and electrochemical impedance spectroscopy (EIS) analyses (see **Figures 19–21**, respectively).

All CV profiles (**Figure 19**) were monitored at a potential window from 0 to 3.5 V at scan rates of 0.05 V s^{-1}. It was clearly seen that the CV curve of EDLC from ACF-AL (EDLC-AL) showed a nearly rectangular shape, while both HKL-based EDLCs showed nearly bow-like profiles. In addition, CV profiles of both HKL-based EDLCs showed peaks at 2.0 – 2.9 V in the charge curve and at 1.2 – 1.8 V in the discharge curve for EDLC-HKL/PEG/CB. The peaks were also observed for the CV profile of EDLC-HKL/PEG at 1.9 – 2.5 V in the charge curve and at 0.7 – 1.3 V in the discharge curve, though the peak area was smaller than those of EDLC-HKL/PEG. In general, such peaks in CV curves result from redox reactions. The detail of the redox reaction will be discussed later in chapter 3.

An electrostatic capacitance was calculated from the area of the CV profile. The area of EDLC-AL had the highest area, which corresponded to the highest electrostatic capacitance of 117.1 F g^{-1}, as shown in **Table 4**. The highest capacitance must be the largest BET surface area of ACF-AL; it was three-fold of those of ACF-HKL/PEG and ACF-HKL/PEG/CB (**Table 3**). The larger surface area, especially the micropore area, could provide more adsorption sites for electrolyte ions, resulting in large electrostatic capacitance. In the case of HKL-based EDLCs, the specific capacitance (88.4 F g^{-1}) for

EDLC- HKL/PEG/CB was larger than that (75.9 F g^{-1}) of EDLC-HKL/PEG. The higher capacitance of EDLC-HKL/PEG/CB was also due to a larger surface area, especially a higher percentage of mesopore size and the external surface area that enabled easy transport of IL ions into the electrode.

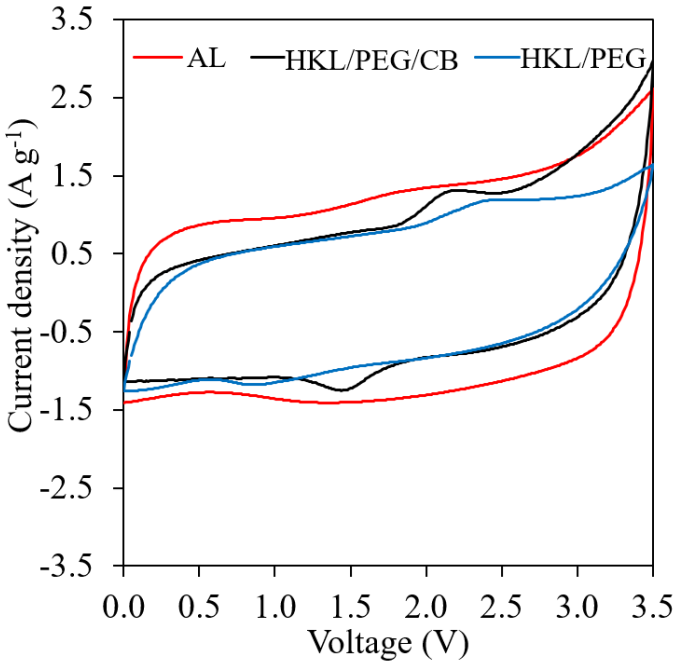

Figure 19. Cyclic voltammograms of the ACFs at 0.05 Vs^{-1}.

Table 4. Electrochemical properties of resultant ACFs at voltage window of 0-3.5 V in ionic liquid electrolyte.

EDLC-samples	C_{sp} [a] (F g^{-1})	C_{sp} [b] (F g^{-1})	R_c [c] (Ω)	R_i [d] (Ω)	V_{drop} (V)	Energy density (Wh kg^{-1})	Power density (kW kg^{-1})
EDLC-KL/PEG	75.9	91.0	2.5	1.9	0.16	39	18
EDLC-KL/PEG/CB	88.4	104.7	2.2	1.8	0.07	45	42
EDLC-AL	117.1	124.2	1.7	1.1	0.03	53	108

[a] Calculated by CV method. [b] Calculated by GCD method.
[c] Charge transfer resistance. [d] Intrinsic resistance.

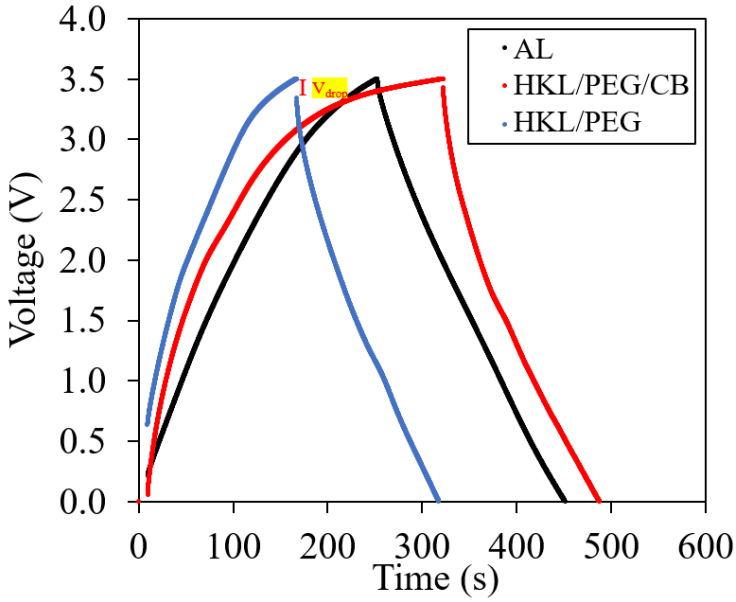

Figure 20. GCD profiles of ACFs at 1 A g^{-1}.

In GCD measurements at a current density of 1 A g^{-1} (**Figure 20**), the profile of EDLC-AL showed a more symmetrical triangle shape than that of HKL-based EDLCs, indicating the more effective formation of the electric double layer. The asymmetrical triangular shape of EDLC-HKL/PEG and EDLC-HKL/PEG/CB indicated a relatively low charge–discharge efficiency. The specific capacitance of EDLC-AL from GCD was calculated from the slope of the discharge line to be 124.2 F g^{-1}, which was also larger than those of EDLC-HKL/PEG (91.0 F/g) and EDLC-HKL/PEG/CB (104.7 F g^{-1}). As shown in **Table 4**, its largest capacitance calculated from the GCD profile of EDLC-AL resulted in the highest energy density (53 Wh kg^{-1}). The largest capacitance and highest energy density of EDLC-AL were, of course, attributed to the large surface area and proper pore size. V_{drop} in the GCD profiles of EDLC-HKL/PEG was significantly greater than that of EDLC-HKL/PEG/CB and EDLC-AL, as shown in **Figure 20**. Since ACFs made from HKL/PEG had the highest surface resistance in section 2.3.3., the huge V_{drop} in EDLC-HKL/PEG is mainly caused by the high electrode resistance. A maximum power density of 108 kW kg^{-1} was accomplished for EDLC-AL with the smallest V_{drop}, because the V_{drop} value was a primary parameter to affect the power density of EDLC.

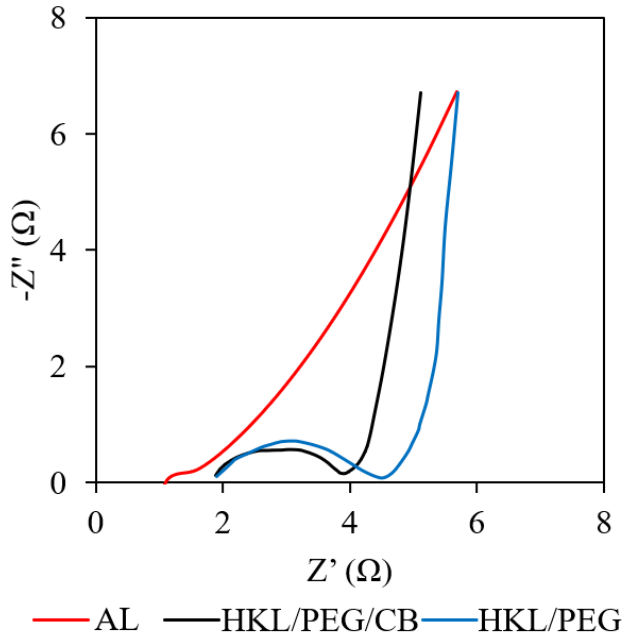

Figure 21. Nyquist plots of ACFs based EDLCs.

Figure 21 shows Nyquist plots of EDLC-HKL/PEG, EDLC-HKL/PEG/CB, and EDLC-AL in a frequency range from 100 kHz to 1 Hz. The semicircle profile of all EDLCs is shown in the high-frequency region or low Z' region. EDLC-AL showed the lowest intrinsic resistance (R_i) of 1.1 Ω among the specimens (EDLC-HKL/PEG was1.9 Ω, and EDLC-HKL/PEG/CB was1.8 Ω). A charge transfer resistance (R_{ct}) of EDLC-AL (1.7 Ω) was also smallest among the specimens (EDLC-HKL/PEG was 2.5 Ω, and EDLC-HKL/PEG/CB was 2.2 Ω), suggesting that the adsorption and desorption rates of the electrolyte onto/from EDLC-AL was fastest than other EDLCs. As mentioned above, the proper size of the electrode pore enhanced the transportation of IL ions, resulting in the reduction of EDLC resistance.

Comparing R_i and R_{ct} between EDLC-HKL/PEG and EDLC-HKL/PEG/CB, the R_i and R_{ct} values of EDLC-HKL/PEG/CB were considerably lower. Obviously, the CB particles in ACF are considered to contribute to the decrease in both resistances.

Thus, in this chapter, the ACFs prepared both from AL and HKL/PEG/CB were demonstrated to be a good electrode material for IL electrolyte because of large surface area, average pore size suitable for IL (**Table 3**), and electrochemical properties of the resultant EDLC (**Table 4**).

The power density and energy density of EDLC assembled with ACFs-AL with IL electrolyte was calculated based on the specific capacitance and applied voltage to be 53 Wh $kg^{-1}$and 108 kW kg^{-1}, respectively. Both energy and power densities obtained in this study were higher than that of EDLC assembled with ACFs-AL with organic electrolyte reported by You et al. (2015b) (42 Wh kg^{-1} and 91 kW kg^{-1}, respectively). This result clearly exhibits an advantage of IL electrolyte over the organic electrolyte due to the wider applied voltage window.

In the preparation of EDLC in this chapter, EDLCs were assembled from the crushed ACFs. I try the direct preparation of EDLC from the ACFs mat without crushing or powdering in the next chapter.

Chapter 3

Preparation of electrode from HKL-based ACFs mat

3.1. Introduction

In the previous chapter, electrodes were prepared from fine particles of ground ACFs. This preparation process required several steps, which were grinding of the ACF mat to powder, mixing with conductive material (*e.g.*, CB) and binder (*e.g.*, sodium carboxymethyl cellulose), casting the resultant mixture on conductive material, and drying for 24 h before EDLC assembly. In this process, the electrode was prepared by remolding of ground ACF mat to the flat sheet. In this chapter, I attempt to directly prepare the electrode from the ACF mat without griding to omit the remolding process involving the grinding, the mixing, and the casting. When the omitting is achieved, the production cost of EDLC is expected to be reduced.

Therefore, an assembly of EDLC is attempted with the ACF mat as electrode material besides the IL electrolyte and the cellulosic separator used in chapter 2, and the electrochemical performance of the resultant EDLC is reported.

3.2. Experimental

3.2.1. Materials

Purified HKL was prepared in the previous chapter. PEG with a molar mass of 500 kDa, acetic acid (AcOH), dimethylformamide (DMF), and hexamethylenetetramine (hexamine; HEX) were purchased from FUJIFILM Wako Pure Chemical Industries, Co, Ltd. (Osaka, Japan). Triethylmethylammonium tetrafluoroborate ($TEMABF_4$) and 1-ethyl-3-methylimidazolium tetrafluoroborate ($EMIBF_4$) were purchased from Tokyo Chemical Industry Co, Ltd. Conductive CB was purchased from Alfa Aesar, Heysham, UK (super P conductive, 99+%). All chemicals were used as received without further purification. An aluminum sheet (0.1 mm in thickness) was purchased from Nilaco Corporation (Tokyo, Japan). Cellulosic separator (type-A sheet) was supplied by Mitsubishi Paper Mills Ltd. (Tokyo, Japan).

3.2.2. Electrospinning of HKL

HKL (1.465 g) and PEG (0.077 g) were mixed at a weight ratio of 95/5, and the mixture was dissolved in a binary solvent (2.5 g) of DMF/AcOH (weight ratio of 6/4) with stirring for 1 h at 80 ^{o}C. HEX (0.441 g) was added to the solution, and it was stirred for 2 h. The electrospinning was carried out under the following conditions. The applied voltage was 18 kV. A positive electrode was connected to the nozzle. Collector was connected to the ground. The distance between the nozzle and collector was 13 cm. The extrusion rate of the solution was about 0.02 mL min^{-1}. The metallic drum collector was wrapped with a sheet of aluminum foil. During the electrospinning of HKL/PEG solution, a 1 wt.% suspension of conductive CB in acetone was sprayed several times on the electrospun fiber mats until the mass of CB reached 1 wt.% and 5 wt.%.

3.2.3. Thermostabilization

The electrospun mat was placed in an electric furnace. The mat was heated from room temperature to 250 ^{o}C at a heating rate of 2 ^{o}C min^{-1} under an air atmosphere, and the temperature was kept for 1 h. After taking out the resultant fiber mat and cooling in air, thermostabilized fibers were obtained.

3.2.4. Carbonization and Activation

The thermostabilized fiber mat was heated in the furnace to 900 ^{o}C at a heating rate of 3 ^{o}C min^{-1} under a nitrogen stream at a flow rate 0.5 L min^{-1}, and the temperature was kept for 1 h. Afterward, steam (19 g) was introduced with a nitrogen stream at a flow rate of 0.5 L min^{-1} to the hot furnace for 1 h. After cooling, activated carbon fibers (ACFs) mat was obtained.

3.2.5. Electrode preparation and EDLC assembly

ACFs mat, aluminum sheets, and a cellulosic separator were cut into circular sheets with a diameter of 16 mm by using a cork borer to yield more than five small sheets for all materials. The two sheets with similar weight (± 0.1 mg) of ACFs mats were selected as a pair of electrodes. The electrodes, the separator, aluminum sheets, and EDLC measurement cell were dried *in vacuo* for 2 h at room temperature. EDLCs were assembled in a two-electrode measurement cell; An aluminum sheet, an ACF mat

electrode, and a cellulosic separator were successively placed at the bottom of the measurement cell. Then, 2–3 drops of the electrolyte were poured on top of the separator. Then, another ACF mat electrode and aluminum sheet were placed on the separator containing the electrolyte. Finally, a stainless-steel disk was placed as a spacer on the aluminum sheet, and the assembled EDLC was tightly pressed using a spring. This assembly process was carried out in a glove box under a N_2 atmosphere. The electrochemical performance of the EDLCs was evaluated by using an electrochemical workstation (Autolab PGSTAT302N FRA32M, Metrohm Autolab) in air and argon atmospheres.

3.3. Characterization

3.3.1. Image and diameter of electrospun fibers and ACFs

The morphology of the fibers was observed under a field emission-scanning electron microscope (FE-SEM; JSM-6301F, JOEL Ltd., Tokyo, Japan) at an accelerating voltage of 5 kV after gold sputtering. Fiber diameter was measured by using a 3-D laser microscope (Violet laser color 3D profile microscope VK-9500, Keyence Japan, Osaka, Japan). At least 5 points for one fiber were measured and the average diameter for the fiber was calculated. The measurement was carried out for at least 20 fibers. Finally, the average diameter of ACFs was obtained from each average diameter of fibers.

3.3.2. Measurements of BET surface area and porosity

The ACF mats were torn by hand into small pieces (about 3x3 mm^2) and heated for 3 h at 297 ^oC in a helium atmosphere. The N_2 adsorption/desorption was measured by using a surface area analyzer (Quantachrome, Autosorb-1) at -196 ^oC. The specific surface areas were calculated from N_2 adsorption isotherms in the relative pressure ($P\ P_0^{-1}$) range of 0.02 to 0.30 by using the BET model. The ratios of the internal to external surface areas in the relative pressure range of 0.2−0.5 $P\ P_0^{-1}$ were calculated according to the *t*-plot method, and the internal and external surface areas were calculated based on the BET surface area and the ratio.

3.3.3. Electrochemical properties of EDLC

The performance of the prepared EDLCs was evaluated by cyclic voltammetry (CV), electrochemical impedance spectroscopy (EIS), and galvanostatic charge/discharge (GCD) method using an electrochemical workstation (Autolab PGSTAT302N FRA32M, Metrohm Autolab B.V.). The specific capacitance (C_s) was calculated from CV and GCD profiles according to equations (3) and (4), respectively. The intrinsic resistance (R_i) and charge transfer resistance (R_{ct}) were obtained from the intercept of impedance in real part (Z_{Re}) and chord length of the simulated impedance circle, respectively, as shown in **Figure 14** in chapter 2.

3.4. Results and Discussion

3.4.1. Electrospun HKL/PEG-based ACF mats

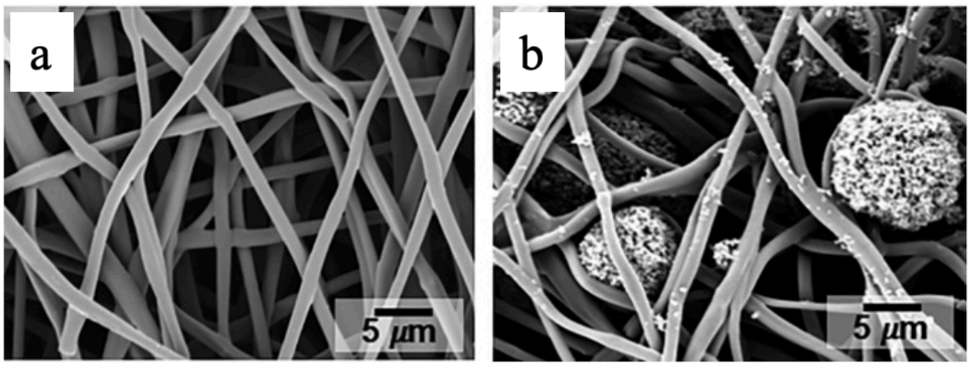

Figure 22. SEM image of ACFs prepared from (a) HKL/PEG and (b) HKL/PEG/5wt%CB

Figure 22-a and -b display microscopic images of ACFs prepared from HKL/PEG and HKL/PEG/5 wt.% CB, respectively. **Figure 22-b** clearly shows the CB particles were embedded between fibers in the ACF mat of HKL/PEG/5 wt.% CB. From **Table 5**, fiber diameters for all electrospun fiber mats were successively decreased by the thermostabilization process and activation process, including the carbonization process. Therefore, each process made fibers thinner. When compared ACF diameters between HKL/PEG, HKL/PEG with 1 wt.% and 5 wt.% CB, the diameter in HKL/PEG mat without CB was smaller than others. The fiber diameter of HKL/PEG/5wt%CB was slightly larger than that of HKL/PEG/1wt%CB. These results demonstrated that the CB spraying gave thicker fibers. An effect of CB addition on pore property in ACFs was investigated from N_2 adsorption/desorption in the next section.

Table 5. Average diameter of electrospun fibers before and after thermostabilization at 2 °C min^{-1} and ACFs.

Samples	Diameter (μm)		
	Thermostabilization		Activation
	Before	After	
HKL/PEG	0.97 ± 0.09	0.76 ± 0.15	0.71 ± 0.10
HKL/PEG/1CB	1.07 ± 0.16	0.95 ± 0.14	0.92 ± 0.10
HKL/PEG/5CB	1.08 ± 0.27	0.97 ± 0.15	0.94 ± 1.60

3.4.2. Determination of surface area and pore volume

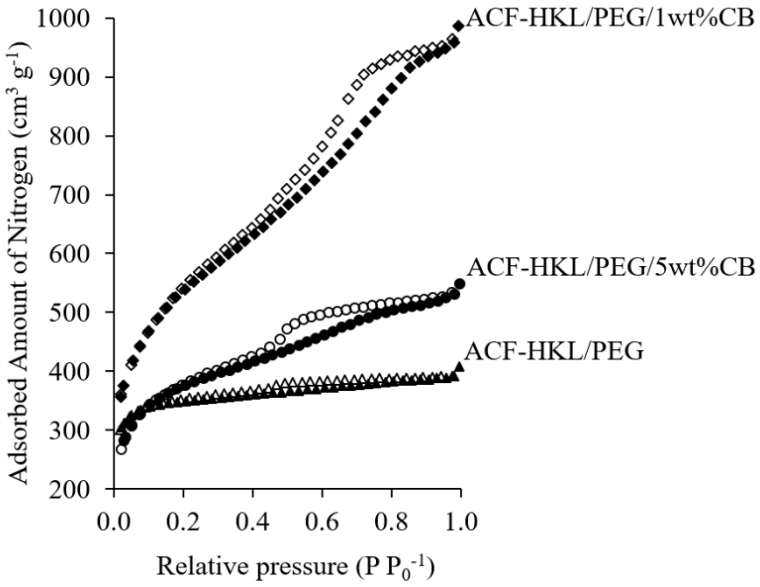

Figure 23. Adsorption (filled symbol) and desorption isotherm (blanked symbol) of ACFs with/without CB.

Figure 23 shows the N_2 adsorption/desorption isotherms of the resultant ACFs. All isotherms showed hysteresis loops, which demonstrated the existence of mesopores in accordance with IUPAC physisorption isotherm recommendations (Sing 1982). The isotherms of ACF-HKL/PEG/1wt%CB and /5wt%CB exhibited larger hysteresis loops, which suggested that mesopores for CB-embedded ACFs had been developed with larger volumes than that of ACF-HKL/PEG.

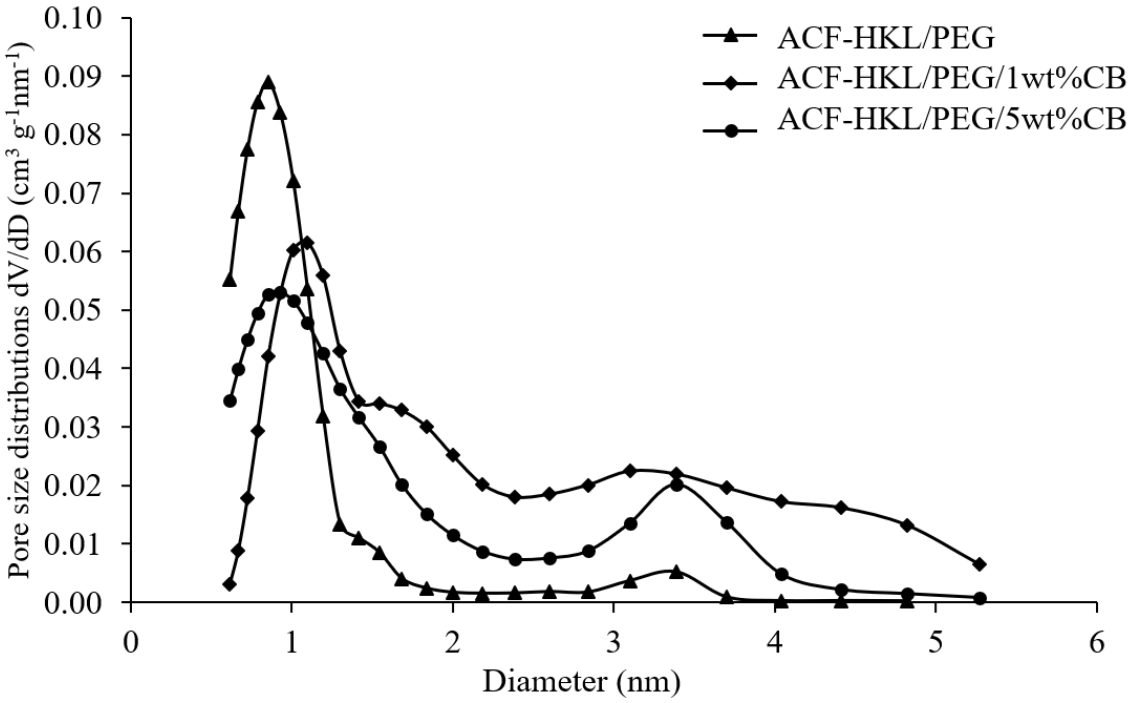

Figure 24. Pore size distribution of ACFs with/without CB.

Table 6. Textural properties of resultant ACFs.

Samples	BET surface area [a] (m^2/g)	Total pore volume [b] (ml/g)	Average pore diameter [b]				Internal surface area [c] (m^2/g)	External surface area [c] (m^2/g)
			Micropore area		Mesopore area			
			(nm)	(%)	(nm)	(%)		
HKL/PEG	1091	0.56	0.89	97.2	2.96	2.8	971	120
HKL/PEG/1CB	1509	1.07	1.17	69.8	3.19	30.2	509	1000
HKL/PEG/5CB	1235	0.75	1.03	84.4	3.04	15.6	798	438

[a] Calculated by the BET model.
[b] Calculated based on QSDFT model.
[c] Calculated according to *t*-plot method.

From **Figure 24** and **Table 6**, all parameter values of the ACFs mat with CB, except for an internal surface area, were larger than that of the ACF mat without CB. This result suggested that CB contributed to the large surface area, pore volume, and pore sizes. The reason is proposed as follows: 1) the embedded CB particles expand the gap between fibers (**Figure 22-b**); 2) the gap allows steam to easily penetrate and diffuse into the gap between fibers, resulting in accelerating activation and generating many pores. When the

CB increased from 1 to 5wt.%, only the internal surface area was increased, although BET surface area was decreased. This may be because the addition of 1 wt.% CB allows the steam to mainly generate the external surface area, which is related to the area of macropore (> 50 nm diameters). As a result, BET surface area was increased. In the case of 5 wt.% CB addition, much CB contributes to the generation of micro- and mesopores but not macropore, resulting in the increase in only the internal surface area.

3.4.3. Electrochemical properties of EDLCs assembled with the ACF mats

3.4.3.1. IL electrolyte stability in a wide voltage window

To confirm the stability of the IL electrolyte in comparison with the organic electrolyte, EDLCs were assembled with ACFs from HKL/PEG together with $TEMABF_4$ as an organic electrolyte and $EMIBF_4$ as IL electrolyte.

In **Figure 25-a**, the CV profiles of EDLC with $TEMABF_4$ at 16–20 scan cycles were fluctuated and did not overlap in the voltage range of 3.0–3.5 V. This result indicated that the organic electrolyte was not stable at high applied voltage. On the other hand, the CV profiles of EDLC with $EMIBF_4$ (**Figure 25-b**) could be overlapped at the scan cycles. Thus, the stability of the IL electrolyte at a wider potential window was confirmed compared to that for the organic electrolyte. A specific capacitance of EDLC-HKL/PEG with the IL electrolyte was estimated from the CV profiles to be about 150 F g^{-1}, which was larger than that (75.9 F g^{-1} in **Table 4**) of EDLC from ground ACF of HKL/PEG. It

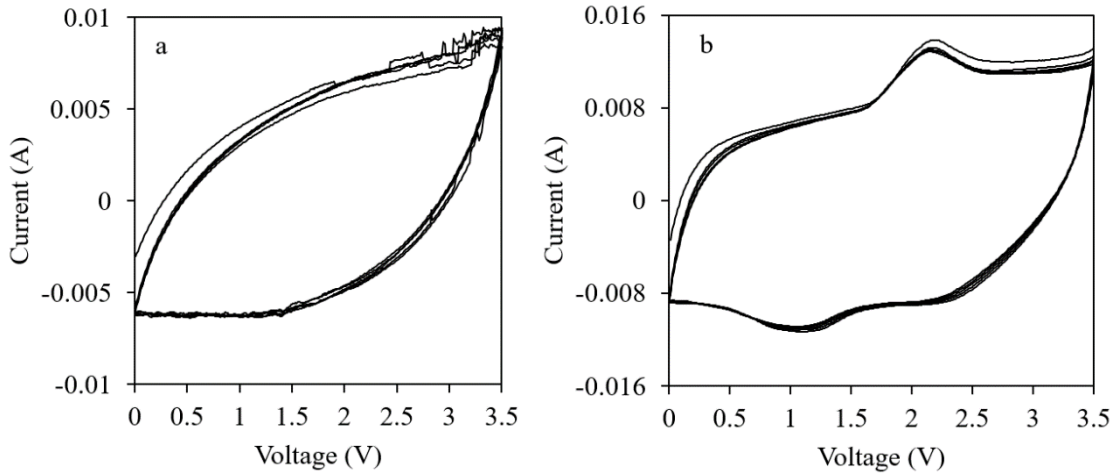

Figure 25. Cyclic voltammograms of EDLC prepared from ACF-HKL/PEG with (a) organic electrolyte solution ($TEMABF_4$/PC) (b) IL electrolyte ($EMIBF_4$) at potential window 0-3.5 V and scan rate 0.05 V s-1 in 16-20 scan cycles.

was anticipated from this result that EDLC from HKL/PEG/5wt% CB exhibited superior performance to EDLC-HKL/PEG because of the larger diameter of micropore (**Table 6**).

3.4.3.2. EDLC with IL electrolyte

EDLCs were assembled with a small circular ACF mat of HKL/PEG/ 1 wt.% CB and /5 wt.% CB as well as the mat of HKL/PEG together with an IL electrolyte ($EMIBF_4$), and a commercial cellulosic separator. The measurements of CV and GCD were operated at 0–3.5 V. CV profiles, GCD profiles, and Nyquist plots for three EDLCs from ACF mats are shown in **Figures 26**, **27**, and **28**, respectively. The parameter values to characterize the electrochemical performance of EDLCs are summarized in **Table 7**.

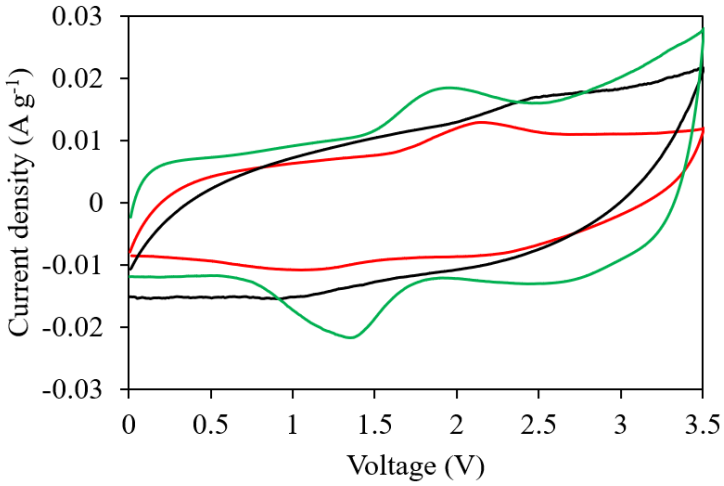

Figure 26. Cyclic voltammograms of ACFs electrode prepared from ACF-HKL/PEG (red), ACF-HKL/PEG/1wt%CB (black) and ACF-HKL/PEG/5wt%CB (green) measured in air at scan rate 0.05 V s^{-1}.

Table 7. Electrochemical properties of resultant ACF mats at voltage window of 0-3.5 V measured in air atmosphere.

EDLC-samples	C_{cv} [a] (F g^{-1})	C_{GCD} [b] (F g^{-1})	R_{ct} [c] (Ω)	R_i [d] (Ω)	Energy density (Wh kg^{-1})	Power density (kW kg^{-1})
EDLC-HKL/PEG	149.8	158.7	16.1	1.6	67.5	11.5
EDLC-HKL/PEG/1wt%CB	114.9	156.3	11.4	1.7	66.5	59.5
EDLC-HKL/PEG/5wt%CB	176.8	227.3	2.8	1.9	91.5	76.2

[a] Calculated by CV method. [b] Calculated by GCD method. [c] Charge transfer resistance
[d] Intrinsic resistance

All CV profiles in **Figure 26** as well as those in **Figure 19** were not rectangular and displayed redox peaks. The reduction peaks appeared around 1.8 V in the green line, around 2.1 V in the red line, and around 2.5 V in the black line, while the oxidation peaks appeared around 1.4 V in the green line, around 1.3 V in the red line, and around 1.1 V in the black line. According to these profiles, the obtained EDLCs were classified as pseudocapacitors rather than simple EDLCs. As shown in **Table 7**, both capacitances (C_{CV} and C_{GCD}) of EDLC-HKL/PEG/5wt%CB were the highest among those of the three EDLCs. The effect of significantly large surface area and high electrical conductivity was assumed to be the reason for the highest capacitance. The BET and internal surface area of ACF mat-HKL/PEG/5wt% CB were the second largest among the specimens, while the conductivity was estimated to be the highest because R_{ct} was the smallest (**Figure 27** and **Table 7**). R_{ct} reflects the conductivity of the electrode: the smaller R_{ct}, the larger conductivity (Lee, 2019). As a result of high capacitance, the EDLC-HKL/PEG/5wt%CB exhibited the highest energy density (91.5 Wh kg^{-1}), which was 2-fold larger than that of the corresponding EDLC from ground ACF-HKL/PEG/5wt%CB and 2.2 times larger than that of EDLC-AL previously reported by You et al. (2015b).

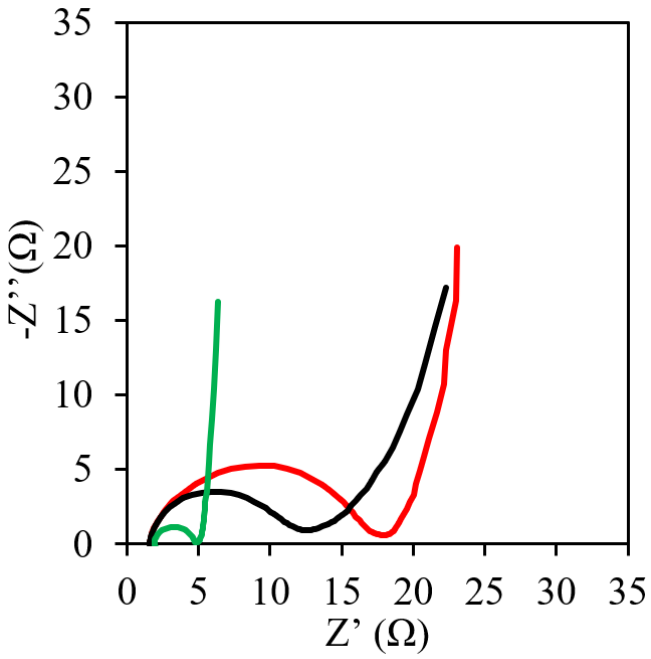

Figure 27. Nyquist plots of electrode prepared from ACF-HKL/PEG (red), ACF-HKL/PEG/1wt%CB (black), and ACF-HKL/PEG/5wt%CB (green).

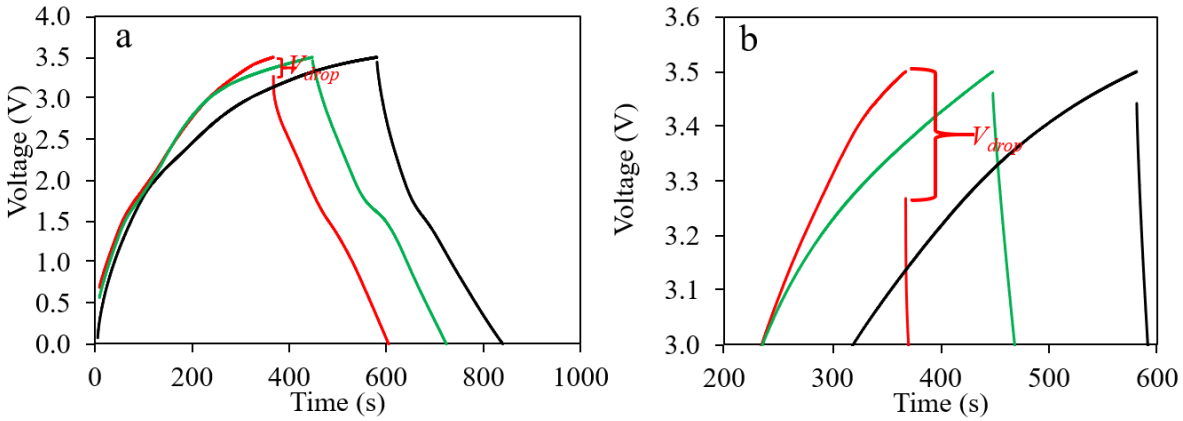

Figure 28. (a) Galvanostatic charge–discharge (GCD) curves of ACF-HKL/PEG (red), ACF-HKL/PEG/1wt%CB (black) and ACF-HKL/PEG/5wt%CB (green) at 0-3.5 V. All samples were measured at current density of 1 A g^{-1} in air (b) the enlarged graph of (a) from 3.0 to 3.5 V.

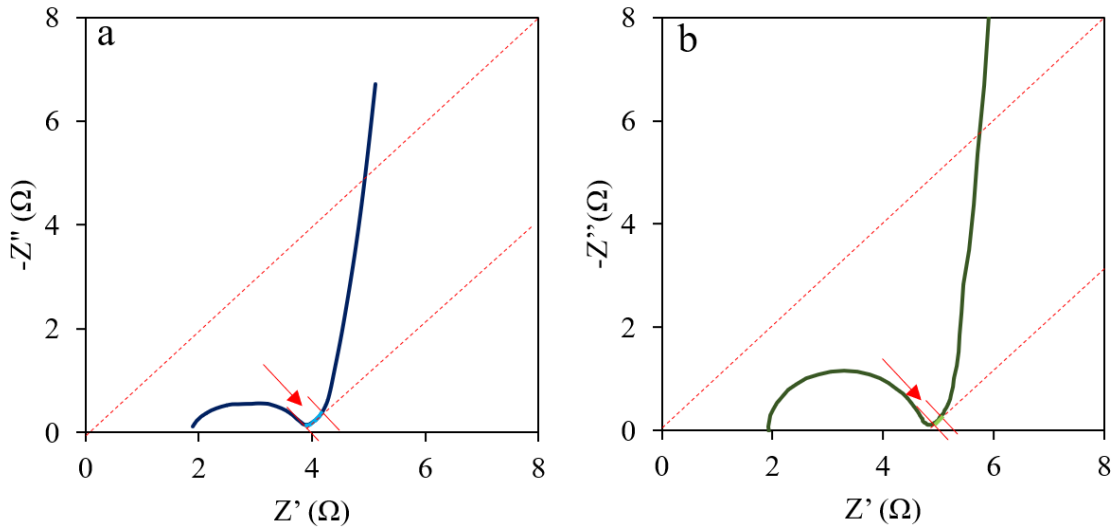

Figure 29. Nyquist plots of the EDLC from (a) ground ACF-HKL/PEG/5wt%CB (b) mat of ACF-HKL/PEG/5wt%CB. The arrows show a diffusion resistance (R_d).

In the GCD profile of **Figure 28**, V_{drop} of EDLC-HKL/PEG/5wt%CB was the smallest among the EDLCs. Since V_{drop} remarkedly affected the power density according to equation (2) in section 1.1, EDLC-HKL/PEG/5wt%CB was revealed to have the highest power density (76.2 kW kg^{-1}), which was about 2-fold larger than the EDLC from ground ACF-HKL/PEG/5wt%CB. The reason for the difference in power density between them must be attributed to diffusion resistance (R_d) (Kumar et al. 2018), which is represented as a difficulty of electrolyte diffusion into the pore of the electrode and can be obtained from the line length of slope at the angle of 45° in a low-frequency region of

Z' in Nyquist plot (Liu et al. 2008), as shown in **Figure 29**. R_d of EDLC from the ACF mat was obviously smaller than that of EDLC from the ground ACF. Thus, R_d is one of the most important resistances to characterize EDLC.

Disappointedly, the power density (91 kW kg^{-1}) was still lower than that of EDLC assembled with AL-based ACF and organic electrolyte in PC (You et al. 2015b). This must be due to the viscosity of the electrolyte, which means the low mobility of the electrolyte. Typically, ionic liquids are more viscous than conventional organic electrolytes (Tachikawa et al. 2010). It is anticipated that electrolytes with low mobility result in a low power density of EDLC.

3.4.3.3. Effect of moisture on redox reaction and cycle life of EDLC

To confirm the durability of EDLC with the IL electrolyte on the cycle of charge/discharge process, GCD of EDLC-HKL/PEG/5wt%CB was measured over 100 cycles, as shown in **Figure 30**. At the 100^{th} cycle, its specific capacitance had decreased from 227.1 F g^{-1} at the 5^{th} scan to 135.1 F g^{-1}, which meant a 40% reduction. Concomitantly, the redox peaks in the CV profiles in **Figure 31-a** were increased as increasing in scan time. It was assumed that the moisture in the air under the measurement conditions of RH 25 ± 3% affected the deterioration of electrode in the EDLC because air easily penetrated into the measurement cell, which was not completely sealed. To investigate the effect of moisture in the EDLC performance, GCD and CV measurements were carried out at RH of 5±2% in the glovebox, which was filled with argon to avoid the air invasion into the cell. The GCD profile measured under a very low humidity showed that the specific capacitance at 100 cycles was 80% on the original capacitance, which was improved by 20% compared to that measured under ambient conditions. In addition, the redox peaks in the CV profile of **Figure 31-b** were markedly decreased in the measurement of low humidity. Therefore, it was proved that moisture affected the deterioration of EDLC performance and redox reaction, which have been already proposed in section 2.3.5 of chapter 2.

In conclusion of this chapter, EDLC with high energy density could be fabricated from HKL/PEG/5wt% CB-ACF mat without grinding; the specific capacitance and energy density were much larger than those of EDLC assembled ground ACF. The reason

could be that the connected structure of fibers facilitated in electrolyte transportation. This achievement will result in a drastic reduction of EDLC production costs.

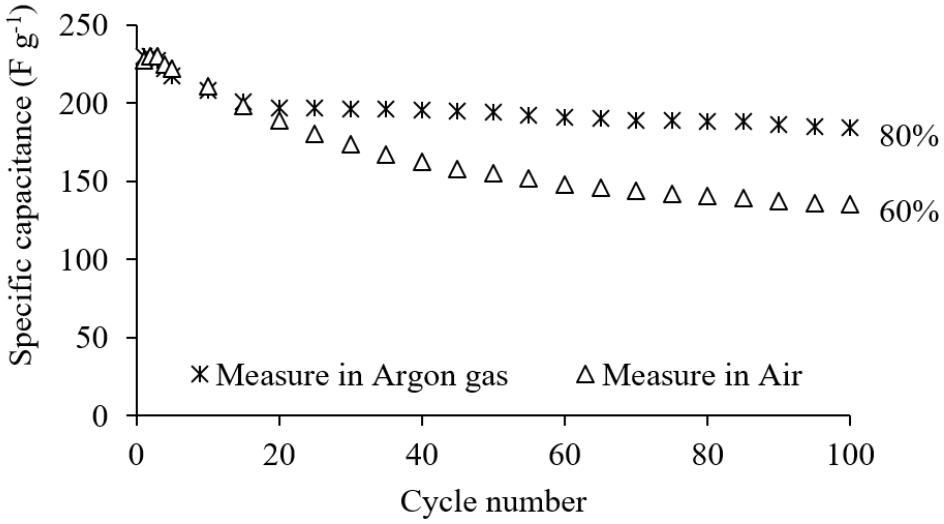

Figure 30. Specific capacitance of EDLC-HKL/PEG/5wt%CB over cycling from GCD at current density of 1 A g^{-1} that measured in air and in argon gas.

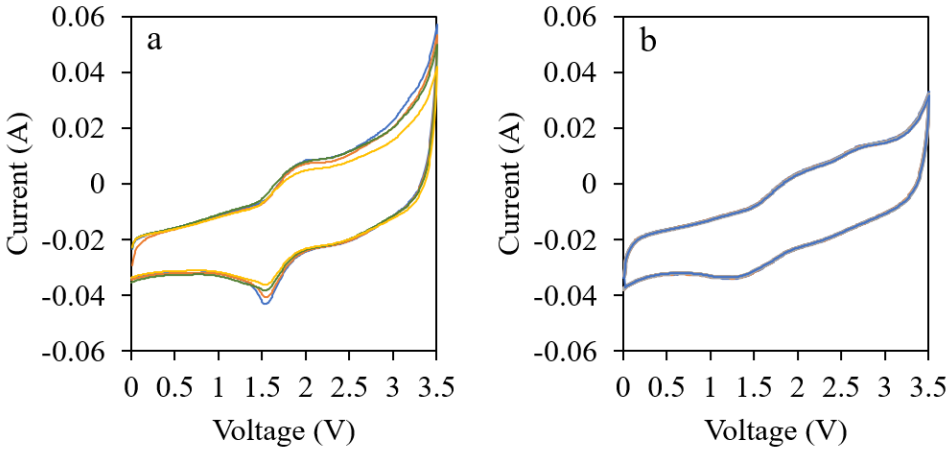

Figure 31. Cyclic voltammograms of EDLC-HKL/PEG/5wt%CB measured for 10 (yellow), 20 (green), 30 (orange), 40 (blue) in air (a) and in argon gas (b).

Chapter 4

Development of lignin-based separator for IL electrolyte

4.1. Introduction

Lignin was used as the main component to prepare electrodes in chapters 2 and 3. However, lignin can be considered a feedstock to prepare other EDLC parts, such as a separator. The laboratory of wood chemistry, which I belong to, developed the lignin-based polyester film (LPF) as a separator for EDLC from binary components of polyethylene glycol lignin (PEGL) and maleic anhydride (MA) (Koda et al. 2019). Polyethylene glycol (PEG) moiety in the lignin skeleton gave PEGL an excellent thermal fusibility (**Figure 32-a**), and hydroxy groups of PEG moieties could readily react with MA to form a network structure of polyester, where the lignin molecules act as crosslinking points (**Figure 32-b**). Since network polymer does not theoretically dissolve in any solvents, the LPF was expected to be a separator for organic electrolytes. However, the electrochemical performance of EDLC was not deteriorated to that of EDLC with a commercial cellulosic separator due to the low flexibility of LPF. To improve its flexibility, PEG with a molar mass of 500 kDa (PEG 500kDa) as a flexible polymer was blended with the LPF prepared from binary components. The EDLC with the resultant LPF from ternary components showed superior flexibility and a similar electrochemical performance to that with cellulosic separator. However, it had a very weak mechanical

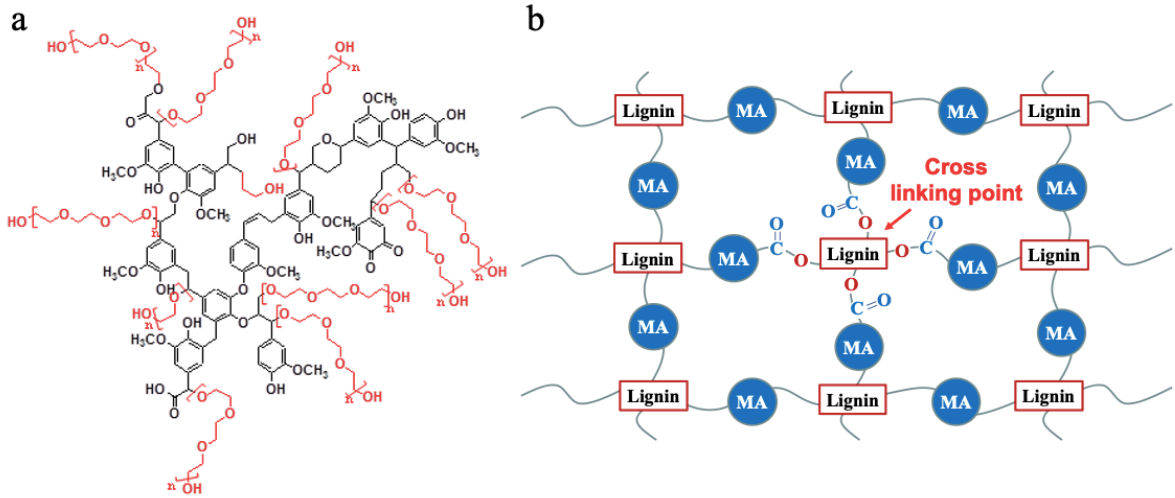

Figure 32. (a) polyethyleneglycol lignin (PEGL) structure (b) network structure of PEGL and maleic anhydride (MA).

strength. The mechanical strength was dramatically improved by the addition of TEMPO-oxidized cellulose nanofiber (TOCN). This film was named quaternary components film, and which kept the flexibility of ternary components, as shown in **Figure 33** (Taira et al. 2019). Furthermore, the film could be converted to the porous one by the addition of NaCl powder followed by washing with water. An EDLC assembled with this film as a separator and the organic electrolyte (1 M $TEMABF_4$/PC) exhibited more excellent electrochemical performance than EDLC with a commercial separator. Thus, it was found that this film was suitable for organic electrolytes, but there is no report on the suitability of this film for IL electrolytes. Therefore, in this chapter, I evaluate this separator suitable for IL electrolytes.

During the above experiment, I have hit upon a good idea on another type of separator, which was an easily prepared electrospun mat. Electrospun mat has many vacant spaces between fibers, which are expected to enable the transportation of IL electrolytes. However, the electrospun mat was easily dissolved in an organic electrolyte. Therefore, thermostabilized electrospun fibers mat, which expected not to dissolve in an electrolyte solution, *i.e.*, $TEMABF_4$ in propylene carbonate (PC). In general, thermostabilized fibers of lignin (Uraki et al. 1995) and polyacrylonitrile fibers (Perananthan et al. 2016) were insoluble in any solvent. Thereby, the thermostabilized electrospun fiber mat of HKL (T-HKL mat) prepared in chapter 2 was considered to be a promising separator for IL electrolytes. An EDLC is also assembled with a T-HKL mat and IL electrolyte, and its electrochemical performance is evaluated.

Figure 33. The LPF prepared from PEGL/MA/PEG500kDa/TOCN

4.2. Experimental

4.2.1. Materials

PEGL was kindly supplied from Harima Chemicals Group, Inc. (Tokyo, Japan), which was prepared from Japanese cedar chips by organosolv pulping with PEG with a molar mass of 400 Da (PEG400) and sulfuric acid (Lin et al. 2012). TOCN aqueous suspension (1% consistency) was supplied from Nippon Paper Industry (Tokyo, Japan). Maleic anhydride (MA), PEG with a molar mass of 500 kDa (PEG 500kDa), acetic acid (AcOH), carbon tetrachloride (CCl_4), *N*,*N*-dimethylformamide (DMF), sodium hydroxide (NaOH), hexamethylenetetramine, sodium carboxymethyl cellulose (CMC), and propylene carbonate (PC, Battery Grade) were purchased from FUJIFILM Wako Pure Chemical Industries, Co, Ltd. (Osaka, Japan). 1-Ethyl-3-methylimidazolium tetrafluoroborate ($EMIBF_4$) and triethylmethylammonium tetrafluoroborate ($TEMABF_4$) were purchased from Tokyo Chemical Industry Co, Ltd. Conductive CB was purchased from Alfa Aesar, Heysham, UK (super P conductive, 99+%). All chemicals were used as received without further purification. An aluminum sheet (0.1 mm in thickness) was purchased from Nilaco Corporation (Tokyo, Japan).

Thermostabilized fibers mat of HKL (T-HKL mat) as a separator was prepared in section 2.2.5 of chapter 2. The electrode prepared from the ground fibers of ACF-AL and ACF-HKL/PEG/5wt%CB in section 2.2.7 of chapter 2, respectively, were used for EDLC assembly in this chapter.

4.2.2. Preparation of LPF from quaternary components

An LPF was prepared according to the previous report (Taira et al. 2019). Briefly, the TOCN aqueous suspension at 1% consistency was mixed with PEG500kDa and PEGL with stirring overnight and lyophilized. The freeze-dried mixture was blended with MA and NaCl powder with a mortar and a pestle and put in a mold prepared from a Teflon sheet, and then covered with another sheet of Teflon (**Figure 34**). The prepared mixture in the mold was subjected to melt-polycondensation at 200 ^{o}C under the pressure of 5 MPa for 4 h, using a hydraulic hot-press machine (HP-300TL-S: Nisshin Science Co. Ltd., Tokyo, Japan). After cooling down, the resulting film was peeled off from the mold and washed with distilled water with shaking at room temperature for 2 days.

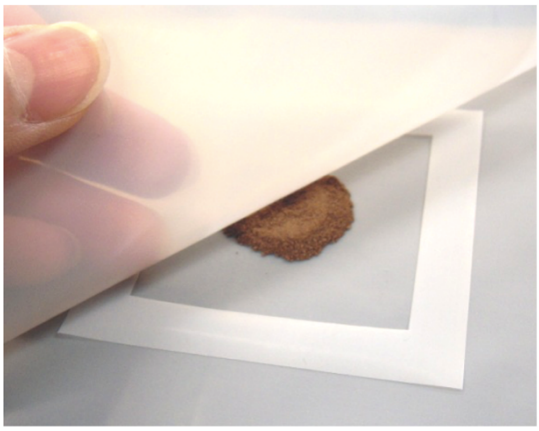

Figure 34. The resultant mixture was set in the Teflon spacer.

4.2.3. Immersion of separators in electrolyte

4.2.3.1. Direct immersion of LPF in the IL electrolyte

An LPF was immersed in $EMIBF_4$ for 3 days and the excess IL electrolyte was removed by wiping the surface of LPF with a filter paper. The weight of LPF was measured before and after the immersion. After the removal of the excess IL electrolyte, the LPF as a separator was subjected to EDLC assembly. The absorption amount of IL electrolyte on LPF was calculated from the weight of the separator before and after immersion by using the following equation:

$$\text{Absorption (g/g)} = \frac{\text{mass of immersed film - mass of dry film}}{\text{mass of dry film}} \quad (10)$$

4.2.3.2. Double immersion of LPF in the organic and IL electrolytes, respectively

An LPF was firstly immersed in the organic electrolyte solution ($TEMABF_4$/PC) for 3 days. The weight of LPF was measured before and after the immersion. Then, the excess organic electrolyte on the LPF surface was removed by a filter paper, and the resultant LPF was also weighed. The LPF was immersed again in $EMIBF_4$ of IL electrolyte for several minutes, and the weight of the resultant LPF was measured. Finally, the LPF was subjected to EDLC assembly.

$$\text{Absorption of } TEMABF_4\text{/PC (g/g) just after immersion (g/g)} = \frac{\text{mass of immersed film in } TEMABF_4\text{/PC - mass of dry film}}{\text{mass of dry film}} \quad (11)$$

Absorption of $TEMABF_4$/PC left in LPF after removal of excess $TEMABF_4$/PC (g/g)

$$= \frac{\text{mass of film after removal - mass of dry film}}{\text{mass of dry film}} \quad (12)$$

Absorption of $EMIBF_4$ (g/g)

$$= \frac{\text{mass of immersed film in } EMIBF_4 \text{ - mass of dry film}}{\text{mass of dry film}} \quad (13)$$

4.2.3.3. Direct immersion of T-HKL mat in IL electrolytes

A T-HKL mat was immersed in IL electrolyte for 3 days. The weight of the LPF was measured before and after the immersion. Then, the excess IL electrolyte was removed by wiping the surface of the mat with a filter paper and the weight of the mat was measured again. After the removal of the excess IL electrolyte, the T-HKL as a separator was subjected to EDLC assembly.

4.2.4. EDLC assembly

EDLC was assembled with electrode prepared in chapter 2 from ground ACF-AL and ACF-HKL/PEG/5wt%CB and the separator of LPF after direct and double immersion and T-HKL mat in accordance with the assembly method described in section 2.2.7 of chapter 2. All the processes for assembly and evaluation of EDLC were carried out under a N_2 atmosphere at very low humidity (RH< 5%) in a glove box.

4.3. Characterization

The morphology of the LPF and the T-HKL mat was observed under a 3-D laser microscope (Violet laser color 3D profile microscope VK-9500, Keyence Japan, Osaka, Japan). The performance of the prepared EDLCs was evaluated by cyclic voltammetry (CV), electrochemical impedance spectroscopy (EIS), and galvanostatic charge/discharge (GCD) method using an electrochemical workstation (Autolab PGSTAT302N FRA32M, Metrohm Autolab B.V.) as well as chapter 2 and 3.

4.4. Results and Discussion

4.4.1. Evaluation of LPF as a separator for IL electrolyte

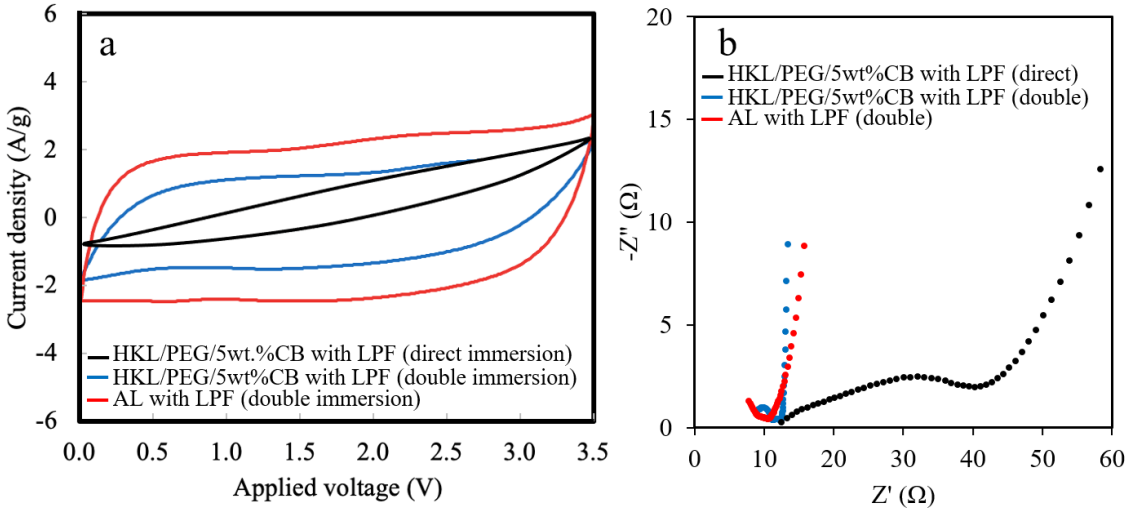

Figure 35. (a) Cyclic voltammogram and (b) Nyquist plot of EDLC assembly with ACFs-based electrode with LPF prepared by direct immersion and double immersion.

As a first attempt to evaluate the LPF as a separator for IL electrolyte, an LPF was simply immersed in $EMIBF_4$ of IL electrolyte and assembly in EDLC with electrode from ground ACF-HKL/PEG/5wt%CB. The electrochemical performance, especially capacitance (C_{cv} = 31 F g^{-1}) and resistances (Ri = 12 Ω, Rct = 65.1 Ω), of the resultant EDLC was very deteriorated to that (C_{cv} = 88.4 F g^{-1}, Ri = 1.8 Ω, Rct = 2.2 Ω) of EDLC assembled with commercial cellulosic separator and the same electrode, as shown in **Figure 35**. The poor electrochemical performance was found to be a small uptake of the electrolyte by the LPF separator.

From the uptake experiment of electrolytes, the LPF absorbed a much larger amount of organic electrolyte solution ($TEMABF_4$/PC) than IL electrolyte ($EMIBF_4$), indicating the high affinity between LPF and $TEMABF_4$/PC. Herein, I hypothesized that both $TEMABF_4$ and $EMIBF_4$ electrolytes should attract each other because they had similar chemical characteristics (*i.e.*, organic quaternary ammonium). Therefore, to achieve uptake of IL by the LPF, I attempted double immersion of the LPF in two electrolytes: First, the LPF was immersed in $TEMABF_4$/PC to form a tight complex, and then the complex immersed in $EMIBF_4$. As a result, the LPF contained 0.45 g/g of organic electrolyte and 0.28 g/g of IL, which was much larger than that (0.05 g/g) obtained from

the direct immersion of LPF in IL electrolyte. Thus, my hypothesis to increase IL uptake was proved.

An LPF prepared via the double immersion was assembled in EDLC together with electrode from ground ACF-HKL/PEG/5wt%CB and ACF-AL. **Figure 35** clearly shows that both of the resultant EDLCs had superior electrochemical performance in both capacitance and resistances to that of EDLC assembled after the direct immersion.

When compared the performance between cellulosic separator and LPF, from **Table 8,** specific capacitances (C_{CV} and C_{GCD}) and energy density (E) of EDLC with the double immersion LPF and ACF-AL were about two times higher than those of EDLC with cellulosic separator. In the case of ACF-HKL/PEG/5wt%CB as an electrode, the performance parameters of EDLC with the LPF was about 1.5 times. The higher capacitance and energy density might be caused by the high mobility of electrolytes, which was explained by (1) the involvement of the carboxy groups of TOCN in LPF and (2) the low viscosity of the mixture composed of IL and organic electrolyte solution, where the organic electrolyte acted as a diluting agent (Guerfi et al. 2010).

However, two drawbacks were found for the EDLCs with double immersion LPF and the two types of electrodes. One was that they had a large V_{drop}, especially for EDLC with ACF-HKL/PEG/5wt%CB, as shown in **Figure 36-a**. Therefore, the EDLCs exhibited much lower power density (7.3 kW kg^{-1} for ACF- HKL/PEG/5wt%CB and 43.5 kW kg^{-1} for ACF-AL) than those of EDLCs with a cellulosic separator (42 kW kg^{-1} for ACF- HKL/PEG/5wt%CB and 108 kW kg^{-1} for ACF-AL). The other drawback was that

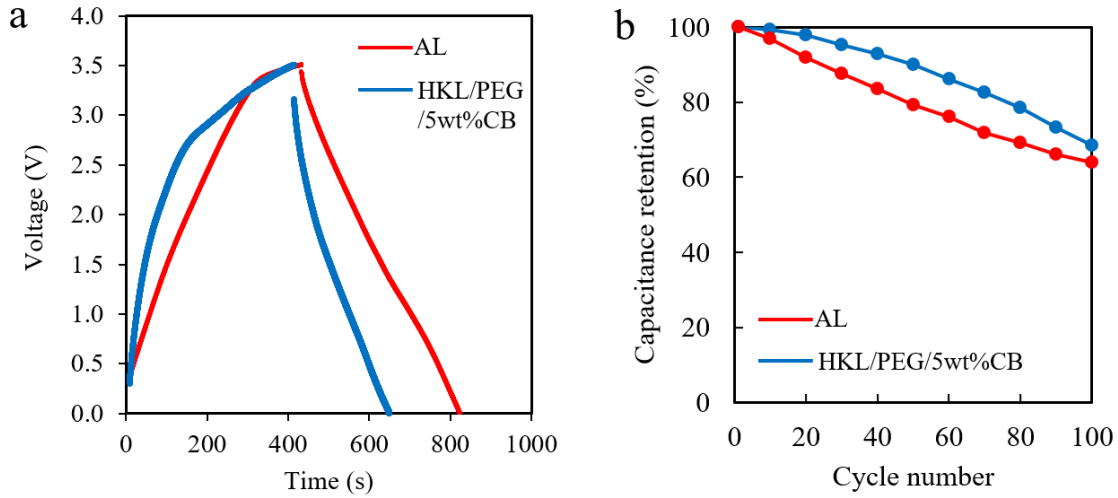

Figure 36. (a) Galvanostatic charge–discharge curves at 0-3.5 V and (b) capacitance retention.

the cycle life of EDLCs was markedly reduced to 60% at 100 cycles on the original capacitance (**Figure 36-b**). These drawbacks might be caused by the porosity of the LPF.

Although the LPF was a porous film, the pore size and the amount of pore would be very small to transport the electrolyte through the film, as shown in **Figure 37**.

Table 8. Electrochemical properties of lignin-based electrode and separator at voltage window of 0-3.5 V measured in argon atmosphere.

EDLC-samples		C_{cv} [a] ($F\ g^{-1}$)	C_{GCD} [b] ($F\ g^{-1}$)	R_{ct} [c] (Ω)	R_i [d] (Ω)	Energy density ($Wh\ kg^{-1}$)	Power density ($kW\ kg^{-1}$)
Electrode	Separator						
HKL/ PEG/ 5wt.%CB	Cellulosic	88.4	104.7	2.2	1.8	45.0	42.0
	LPF [e]	107.4	150.4	3.8	8.4	64.0	7.3
	T-HKL/PEG mat	90.7	114.3	1.2	1.9	48.6	178.4
AL	Cellulosic	117.1	124.2	1.7	1.1	53.0	108.0
	LPF [e]	182.4	238.1	2.1	6.2	101.3	43.5
	T-HKL/PEG mat	159.2	181.8	0.5	1.8	77.3	110.0

[a] Calculated by CV method. [b] Calculated by GCD method. [c] Charge transfer resistance
[d] Intrinsic resistance [e] LPF prepared from double immersion technique

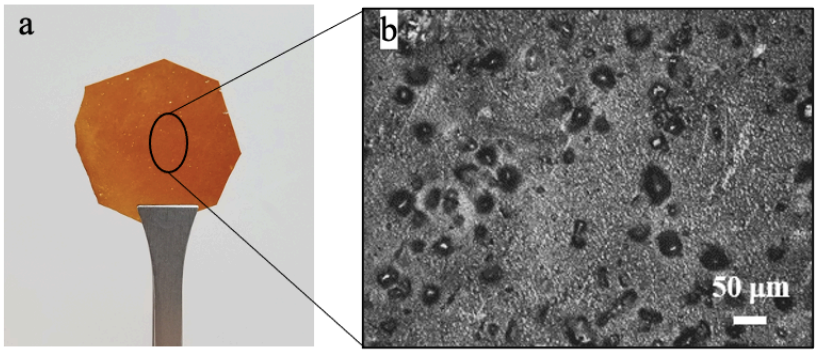

Figure 37. (a) optical photograph (b) microscopic images of LPF with porous morphology.

4.4.2. Evaluation of T-HKL mat as a separator for IL electrolyte

As an alternative porous material to LPF, the thermostabilized electrospun fibers mat was considered to be a good candidate for EDLC separator because it has a high vacant space between fibers (**Figure 38**) in which the electrolyte molecules can easily move. In addition, it cannot be dissolved in the IL electrolyte due to a crosslinking structure.

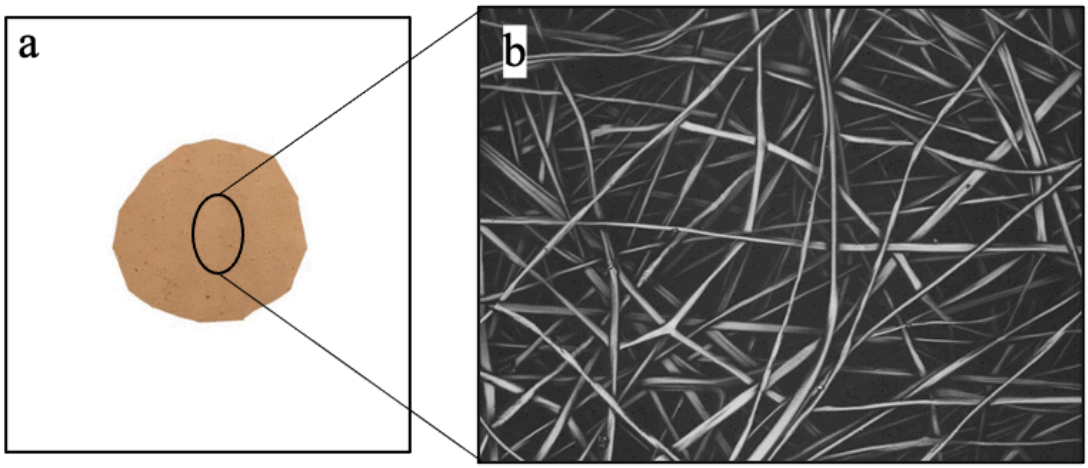

Figure 38. (a) optical photograph (b) microscopic images of T-HKL/PEG mat.

EDLC with T-HKL mat was assembled with the same two types of electrodes and the electrolyte as the EDLC with the LPF. The power density of EDLCs with T-HKL mat was much higher than that of EDLC with LPF, although the capacitance and energy density were lower than EDLC with LPF (**Figure 39**, **40-a,** and **Table 8)**. In addition, C_{GCD} retention of EDLCs with T-HKL mat at 100 cycles was 80% on the original capacitance (**Figure 40-b**), which was improved by 20% compared to those of EDLCs with LPF. As expected, EDLCs with T-HKL mat had a higher power density than those of EDLCs with LPF. However, their capacitance and energy density were lower. Although the T-HKL mat was a highly porous material resulting in easy transportation of

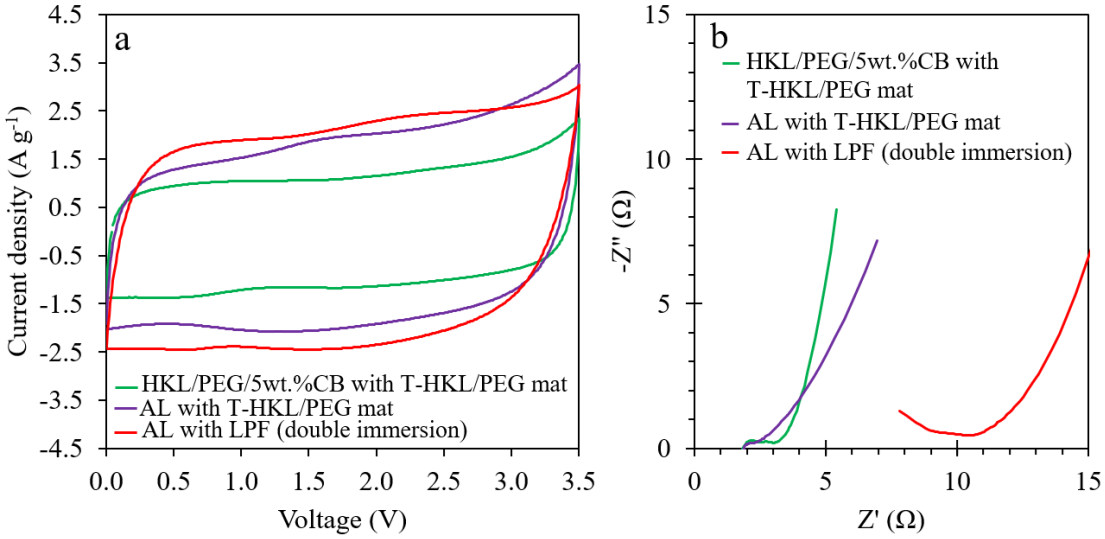

Figure 39. (a) Cyclic voltammogram and (b) Nyquist plot of EDLC assembled with electrode from ACFs and separator from T-HKL/PEG mat and LPF (double immersion).

electrolytes, there were no functional groups such as carboxylic groups that facilitate the transport of electrolytes as in LPF. Therefore, lower capacitance and energy density of EDLC with T-HKL mat were obtained.

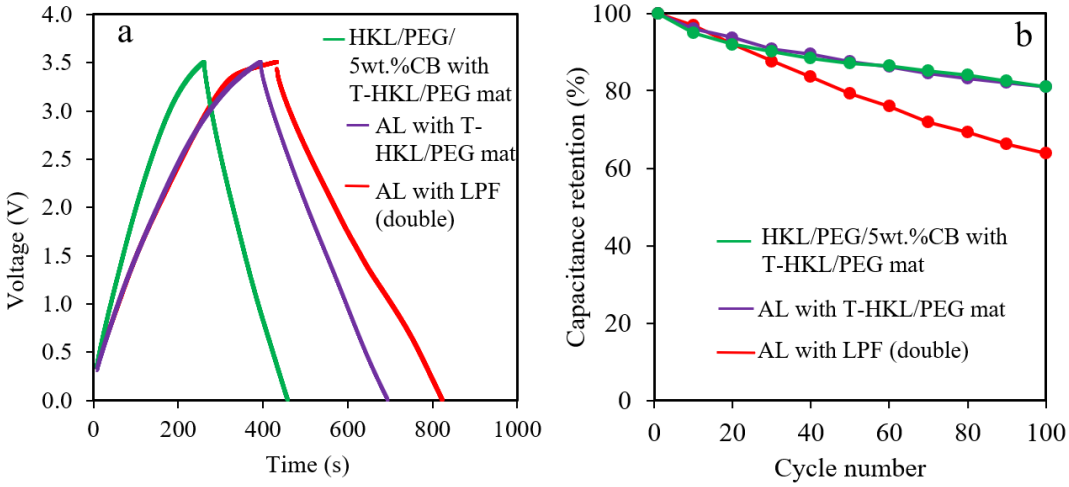

Figure 40. (a) Galvanostatic charge–discharge curves at 0-3.5 V and (b) capacitance retention (in percentage) of EDLC assembly with electrode from ACFs and separator from T-HKL/PEG mat and double immersion LPF.

When compared T-HKL mat with cellulosic separator, two EDLCs with T-HKL mat had superior parameters values of electrochemical performance to the corresponding EDLCs with a cellulosic separator (**Table 8**). This might be because the transportation of electrolytes through the T-HKL mat was easier than the cellulosic separator due to a larger vacant space between fibers in the T-HKL mat than that of the cellulosic separator, as shown in **Figure 41**. Thus, the superior separator to commercial cellulosic separator was successfully prepared from the electrospun mat of HKL.

In this chapter, I demonstrated that EDLC parts including electrode and separator could be produced by lignin. Moreover, both lignin-based electrode and separator could enhance the electrochemical performance of EDLC.

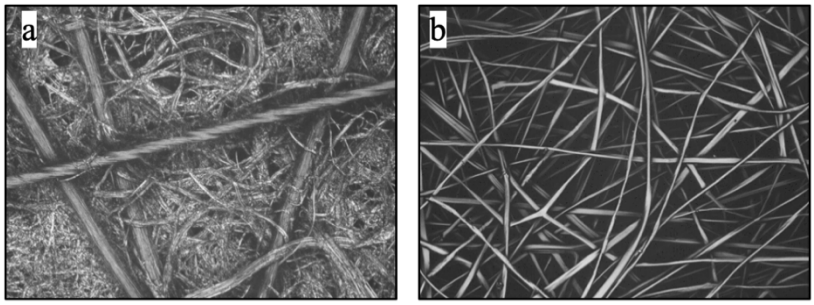

Figure 41. Microscopic images of (a) cellulosic separator (b) T-HKL mat.

Chapter 5

5.1. Concluding remarks

An objective of this study was to prepare an electric double layer capacitor (EDLC) with high energy density mainly from technical lignins as a novel utilization field of lignins isolated from wood. To achieve the objective, I focused on ionic liquid (IL) electrolytes because they are available at a very wide operating voltage, providing enhanced energy density. Therefore, EDLC parts, an electrode and a separator, suitable for an IL electrolyte were attempted to be developed from several technical lignins. Major findings and achievement in this study are summarized as follows:

From Chapter 2,

1) I assumed that acetic acid lignin (AL)-based ACF was a promising material to prepare electrode suitable for the IL electrolyte from the pore size reported previously (You et al. 2015b). As a first attempt, I assembled EDLC with AL-ACF particles obtained by grinding the AL-ACF mat, carbon black (CB), a commercial separator, and an IL electrolyte (1-ethyl-3-methylimidazolium tetrafluoroborate, $EMIBF_4$) and evaluated its electrochemical performance. As expected, the energy density (53 Wh kg^{-1}) of the EDLC was larger than that (42 Wh kg^{-1}) of EDLC with organic electrolyte.

From Chapter 2 and 3,

2) Hardwood kraft lignin (HKL) can be easily obtained than AL because kraft pulping is a major chemical pulping worldwide. Therefore, the main objective of my study was to fabricate EDLC suitable for IL electrolytes mainly from HKL-derived materials. As a second attempt, an EDLC electrode was prepared from HKL.

At first, the electrode was prepared from HKL-ACF particles obtained by grinding the HKL-ACF mat as well as the electrode preparation from AL. Unfortunately, the energy density (39 Wh kg^{-1}) of the resultant EDLC with HKL-ACF particles was low. The energy density was improved by the modification of the HKL electrospinning: CB was sprayed onto the HKL mat during the electrospinning. However, the energy density (45 Wh kg^{-1}) was still lower than that of AL-based EDLC.

If the electrochemical performance of EDLC from HKL could not be improved, I thought that the production cost should be reduced to expand the utilization of HKL. Very fortunately, the EDLC with the highest energy density (91.5 Wh kg^{-1}) was successfully fabricated from HKL as follows: The CB was sprayed on the HKL mat during electrospinning, and the resultant mat was converted to an ACF mat. The ACF mat without grinding was directly inserted as an electrode into EDLC. In the assembly, the IL electrolyte was just dropped on the separator instead of soaking a separator and electrodes in the IL electrolyte. Thus, this procedure omitted the grinding process of the ACF mat and soaking process of EDLC parts, resulting in the reduction of production cost and time.

From Chapter 4,

3) Lignin-based polyester film (LPF), previously reported by Taira et al. (2019), had been a suitable separator for an organic electrolyte. Although the LPF was directly used as a separator for IL electrolyte in this study, the resultant EDLC showed a very poor electrochemical performance. However, the performance could be improved by the modification of the soaking process, in which the LPF was successively soaked in an organic electrolyte and IL electrolyte. By this double soaking, the resultant EDLC showed 64 Wh kg^{-1} of energy density, which was superior to that of EDLC with cellulosic separator as a positive control.

4) I considered the thermostabilized electrospun fiber mat as an alternative separator because it resisted dissolution in any solvents and had much vacant space. Thereby, EDLC was assembled with a thermostabilized fibers mat of HKL (T-HKL mat) instead of a cellulosic separator together with ground particles of HKL-ACF as an electrode material. The resulting EDLC with T-HKL mat exhibited the highest power density (178.4 kW kg^{-1}) among all EDLCs prepared in this study, whereas its energy density was lower than that of EDLC with a doubly soaked LPF separator.

In this study, several types of lignin were utilized as a raw material to produce electrodes and a separator in EDLC with excellent electrochemical performance. Especially, the utilization of kraft lignin was demonstrated. Thereby, lignin-based EDLC

would be viable in the near future. Furthermore, I am convinced that the achievements in this study will impact not only the utilization of lignin in a new application field, leading to the sustainable development of pulping industry, but also constructing a sustainable supply system of electricity based on renewable energy. Finally, this research will contribute to the creation of a society, which does not depend on fossil resources.

5.2. Perspective in the near future

This study demonstrated that lignin could be utilized as an electrode (Pakkang et al. 2020) and separator parts in EDLC. Another important organic part in EDLC is an electrolyte. When electrolytes can be produced from natural or renewable materials instead of fossil resources, all EDLC parts are fabricated from bio-based materials.

Ionic liquid (IL) electrolyte can be classified into two types based on cation structure: one is imidazolium type, and the other one is a type of quaternary alkyl ammonium with long alkyl chains (Aldroubi et al. 2021). It is likely to be difficult to prepare both types of IL electrolytes from lignin. However, the quaternary alkylammonium type of IL may be prepared from natural compounds such as plant oil and terpenoid, although imidazolium type of IL ($EMIBF_4$) is used in this study.

I focused on plant oils as a feedstock to produce quaternary alkyl ammonium type of IL. This is because the plant oil contains glycerides comprised of fatty acids with a long alkyl chain and glycerol. Fatty acids are a promising raw material to prepare the IL. Fatty acids can be directly used as an anion part in the IL electrolyte. Moreover, it can be converted to cation part of IL electrolyte as follows: (i) the acid can be converted to alkyl halide (R-Cl) via three steps; (ii) R-Cl is coupled with mono-, di- and tri-alkyl amines to produce quaternary alkylammoniums with the different number of long alkyl chain (R). The viscosity of IL must be controlled by changing the number of R. Among natural fatty acids, ricinoleic acid from castor oil and linoleic acid from sunflower oil are considered the most promising because ricinoleic acid has a hydroxy group, and linoleic acid has two double bonds in their alkyl chains in addition to their abundance in nature. As a preliminary experiment to get fundamental information on their chemical properties, I investigated the Zeta (ζ) Potential and emulsion formation in the presence of water (Pakkang et al. 2018). The results showed that both oils had higher electric potential in

the presence of water. Therefore, I consider these fatty acids are attractive materials to produce IL electrolytes. As my next research, the conversion of fatty acids to cationic parts is the main topic. The success of this research will contribute to not only the development of bio-based EDLC but also the creation of a sustainable society based on renewable energy.

References

Aldroubi, S., Brun, N., Bou Malham, I., & Mehdi, A. (2021). When graphene meets ionic liquids: a good match for the design of functional materials. Nanoscale, 13(5), 2750–2779.

Alonso, D.M., Wettstein, S.G., & Dumesic, J.A. (2012). Bimetallic catalysts for upgrading of biomass to fuels and chemicals. Chemical Society Reviews, 41(24), 8075–8098.

Alzagameem, A., Klein, S., Bergs, M., Do, T., Korte, I., Dohlen, S., Hüwe, C., Kreyenschmidt, J., Kamm, B., Larkins, M., & Schulze, M. (2019). Antimicrobial activity of lignin and lignin-derived cellulose and chitosan composites against selected pathogenic and spoilage microorganisms. Polymers, 11(4), 670.

Arapova, O.V., Chistyakov, A.V., Tsodikov, M.V., & Moiseev, I.I. (2020). Lignin as a renewable resource of hydrocarbon products and energy carriers (A Review). Petroleum Chemistry, 60(3), 227–243.

Baker D.A. & Rials T.G. (2013). Recent advances in low-cost carbon fiber manufacture from lignin. Journal of Applied Polymer Science, 130(2), 713–728.

Baker, D.A., Gallego, N.C., & Baker, F.S. (2012). On the characterization and spinning of an organic-purified lignin toward the manufacture of low-cost carbon fiber. Journal of Applied Polymer Science, 124(1), 227-234.

Bengtsson, J., Jedvert, K., Köhnke, T., & Theliander, H. (2019). Identifying breach mechanism during air-gap spinning of lignin–cellulose ionic-liquid solutions. Journal of Applied Polymer Science, 136(30), 47800.

Bennani, A., Rigal, L., & Gaset, A. (1991). Refining of lignocellulose by organosolv processes. Part I: Isolation, characterisation and utilization of hemicellulose extracted from Norway spruce. Biomass and Bioenergy, 1(5), 289-296.

Braun, J., Holtman, K., & Kadla, J. (2005). Lignin-based carbon fibers: Oxidative thermostabilization of kraft lignin. Carbon, 43(2), 385-394.

Burke, A. (2007). R&D considerations for the performance and application of electrochemical capacitors. Electrochimica Acta, 53(3), 1083-1091.

Chand, S. (2000). Review carbon fibers for composites. Journal of Materials Science, 35, 1303-1313.

Chmiola, J. (2006). Anomalous increase in carbon capacitance at pore sizes less than 1 nanometer. Science, 313(5794), 1760-1763.

Cole, B.J.W., Huth, S.P., & Runnels, P.S. (1993). Modification of high-yield pulps with polyethylene glycols. I. Model compound and isolated lignin studies. Journal of Wood Chemistry and Technology, 13(1), 59–72.

Daniyan, I.A., Mpofu, K., Adeodu, A.O., & Adesina, O. (2020). Development of carbon fibre reinforced polymer matrix composites and optimization of the process parameters for railcar applications. Materials Today: Proceedings, 38(2), 628-634.

Daraghmeh, A., Hussain, S., Saadeddin, I., Servera, L., Xuriguera, E., Cornet, A., & Cirera, A. (2017). A study of carbon nanofibers and active carbon as symmetric supercapacitor in aqueous electrolyte: a comparative study. Nanoscale Research Letters, 12, 639.

Dold, C., Henerichs, M., Bochmann, L., & Wegener, K. (2012). Comparison of ground and laser machined polycrystalline diamond (PCD) tools in cutting carbon fiber reinforced plastics (CFRP) for aircraft structures. Procedia CIRP, 1, 178–183.

Dorrestijn, E., Laarhoven, L.J.J., Arends, I.W.C.E., & Mulder, P. (2000). The occurrence and reactivity of phenoxyl linkages in lignin and low rank coal, Journal of Analytical and Applied Pyrolysis, 54(1-2), 153-192.

Fang, W., Yang, S., Wang, X.L., Yuan, T.Q., & Sun, R.-C. (2017). Manufacture and application of lignin-based carbon fibers (LCFs) and lignin-based carbon nanofibers (LCNFs). Green Chemistry, 19(8), 1794-1827.

Fitzer, E. & Müller, D.J. (1975). The influence of oxygen on the chemical reactions during stabilization of pan as carbon fiber precursor. Carbon, 13(1), 63-69.

Föllmer, M., Jestin, S., Neri, W., Vo, V.S., Derré, A., Mercader, C., & Poulin, P. (2019). Wet-spinning and carbonization of lignin-polyvinyl alcohol precursor fibers. Advanced Sustainable Systems, 3(11), 1900082.

Gao, Q., Demarconnay, L., Raymundo-Piñero, E., & Béguin, F. (2012). Exploring the large voltage range of carbon/carbon supercapacitors in aqueous lithium sulfate electrolyte. Energy & Environmental Science, 5, 9611-9617.

Guerfi, A., Dontigny, M., Charest, P., Petitclerc, M., Lagacé, M., Vijh, A., & Zaghib, K. (2010). Improved electrolytes for Li-ion batteries: Mixtures of ionic liquid and

organic electrolyte with enhanced safety and electrochemical performance. Journal of Power Sources, 195(3), 845–852.

Hayyan, M., Mjalli, F.S., Hashim, M.A., AlNashef, I.M., & Mei, T.X. (2013). Investigating the electrochemical windows of ionic liquids. Journal of Industrial and Engineering Chemistry, 19(1), 106–112.

Hu, S., Zhang, S., Pan, N., & Hsieh, YL. (2014). High energy density supercapacitors from lignin derived submicron activated carbon fibers in aqueous electrolytes. Journal of Power Sources, 270, 106-112.

Huang, Y., & Zhao, G. (2016). Preparation and characterization of activated carbon fibers from liquefied wood by KOH activation. Holzforschung, 70(3), 195–202.

Inagaki, M., Konno, H., & Tanaike, O. (2010). Carbon materials for electrochemical capacitors. Journal of Power Sources, 195(24), 7880-7903.

Jayawickramage, R.A.P., Balkus, K.J., & Ferraris, J.P. (2019). Binder free carbon nanofiber electrodes derived from polyacrylonitrile-lignin blends for high performance supercapacitors. Nanotechnology, 30, 355402.

Jonglertjunya, W., Juntong, T., Pakkang, N., Srimarut, N., & Sakdaronnarong, C. (2014). Properties of lignin extracted from sugarcane bagasse and its efficacy in maintaining postharvest quality of limes during storage. LWT - Food Science and Technology, 57(1), 116-125.

Kadla, J.F., Kubo, S., Venditti, R.A., Gilbert, R.D., Compere, A.L., & Griffith, W. (2002). Lignin-based carbon fibers for composite fiber applications. Carbon, 40(15), 2913-2920

Koda, K., Taira, S., Kubota, A., Isozaki, T., You, X., Uraki, Y., Sugimura, K., & Nishio, Y. (2019). Development of lignin-based terpolyester film and its application to separator material for electric double-layer capacitor. Journal of Wood Chemistry and Technology, 39(3), 198-213.

Kubo, S., Uraki, Y., & Sano, Y. (1998). Preparation of carbon fibers from softwood lignin by atmospheric acetic acid pulping. Carbon, 36(7-8), 1119-1124.

Kumar, M., Hietala, M., & Oksman, K. (2019). Lignin-based electrospun carbon nanofibers. Frontiers in Materials, 6(62), 1-6.

Kumar, P., Bharti, R.P., Kumar, V., & Kundu, P.P. (2018). Polymer electrolyte membranes for microbial fuel cells: Part A. Nafion-based membranes. In P.P. Kundu & K. Dutta (Eds.), Progress and Recent Trends in Microbial Fuel Cells (pp. 47–72). Elsevier.

Largeot, C., Portet, C., Chmiola, J., Taberna, P.-L., Gogotsi, Y., & Simon, P. (2008). Relation between the ion size and pore size for an electric double-layer capacitor. Journal of the American Chemical Society, 130(9), 2730–2731.

Leahy, S. (2021, February 10). We have too many fossil-fuel power plants to meet climate change goals. Retrieved April 25, 2021, from https://www.nationalgeographic.com/environment/article/we-have-too-many-fossil-fuel-power-plants-to-meet-climate-goals.

Lee, Y. (2019). The effect of active material, conductive additives, and binder in a cathode composite electrode on battery performance. Energies, 12(4), 658.

Lin J., Koda K., Kubo S., Yamada T., Enoki M., & Uraki Y. (2013). Improvement of mechanical properties of softwood lignin-based carbon fibers. Journal of Wood Chemistry andogy Technol, 34(2), 111-121.

Lin J., Kubo S., Yamada T., Koda K., & Uraki Y. (2012). Chemical thermostabilization for the preparation of carbon fibers from softwood lignin. BioResources, 7(4), 5634-4646.

Liu, C.L., Dong, W.S., Cao, G.P., Song, J.R., Liu, L., & Yang, Y.S. (2008). Capacitance limits of activated carbon fiber electrodes in aqueous electrolyte. Journal of The Electrochemical Society, 155(1), F1–F7.

Liu, Z., Huang, Y., & Zhao, G. (2016). Preparation and characterization of activated carbon fibers from liquefied wood by $ZnCl_2$ Activation. BioResources, 11(2), 3178-3190.

Mainka, H., Täger, O., Körner, E., Hilfert, L., Busse, S., Edelmann, F.T., & Herrmann, A.S. (2015). Lignin-an alternative precursor for sustainable and cost-effective automotive carbon fiber, Journal of Materials Research and Technology, 4(3), 283-296.

Martín, C., Ronda, J. C., & Cádiz, V. (2006). Development of novel flame-retardant thermosets based on boron-modified phenol–formaldehyde resins. Journal of Polymer Science Part A: Polymer Chemistry, 44(11), 3503-3512.

Mhamane, D., Suryawanshi, A., Banerjee, A., Aravindan, V., Ogale, S., & Srinivasan, M. (2013). Non-aqueous energy storage devices using graphene nanosheets synthesized by green route. AIP Advances, 3(4), 042112.

Mousavi, M.P.S., Wilson, B.E., Kashefolgheta, S., Anderson, E.L., He, S., Bühlmann, P., & Stein, A. (2016). Ionic liquids as electrolytes for electrochemical double-layer capacitors: structures that optimize specific energy. ACS Applied Materials & Interfaces, 8(5), 3396–3406.

Nikoloutsopoulos, N., Passa, D., Gavela, S., & Sotiropoulou, A. (2018). Comparison of shear strengthening techniques of reinforced concrete beams with carbon fibre reinforced polymers (CFRPs). Procedia Structural Integrity, 10, 141–147.

Pakkang, N., Kumar, M., Taira, S., Koda, K., Shigetomi, K., & Uraki, Y. (2020). Preparation of kraft lignin-based activated carbon fiber electrodes for electric double layer capacitors using an ionic liquid electrolyte. Holzforschung, 74(6), 577-588.

Pakkang, N., Uraki, Y., Koda, K., Nithitanakul, M., & Charoensaeng, A. (2018). Preparation of Water-in-Oil Microemulsion from the Mixtures of Castor Oil and Sunflower Oil as Makeup Remover. Journal of Surfactants and Detergents, 21(6), 809–816.

Pandit, B., Dubal, D.P., & Sankapal, B.R. (2017). Large scale flexible solid state symmetric supercapacitor through inexpensive solution processed V_2O_5 complex surface architecture. Electrochimica Acta, 242, 382–389.

Park, J.H., Rana, H.H., Lee, J.Y., & Park, H.S. (2019). Renewable flexible supercapacitors based on all-lignin-based hydrogel electrolytes and nanofiber electrodes. Journal of Materials Chemistry A, 7(28), 16962–16968.

Perananthan, S., Bonso, J. S., & Ferraris, J. P. (2016). Supercapacitors utilizing electrodes derived from polyacrylonitrile fibers incorporating tetramethylammonium oxalate as a porogen. Carbon, 106, 20–27.

Pohlmann, S. (2017, July 4). What is A Pseudocapacitor? - Capacitors explained. Retrieved April 29, 2021, from https://www.skeletontech.com/skeleton-blog/what-is-a-pseudocapacitor-capacitors-explained.

Qu, D. & Shi, H. (1998). Studies of activated carbons used in double-layer capacitors. Journal of Power Sources, 74(1), 99-107.

Ravikovitch, P.I., Domhnaill, S.C., Neimark, A.V., Schueth, F., & Unger, K.K. (1995). Capillary hysteresis in nanopores: Theoretical and experimental studies of nitrogen adsorption on MCM-41. Langmuir, 11(12), 4765-4772.

Roman, J., Neri, W., Derré, A., & Poulin, P. (2019). Electrospun lignin-based twisted carbon nanofibers for potential microelectrodes applications. Carbon, 145, 556-564.

Sadeghifar, H., & Ragauskas, A. (2020). Lignin as a UV light blocker—A Review. Polymers, 12(5), 1134.

Sánchez-Montero, M. J., Salvador, F., & Izquierdo, C. (2008). Reactivity and porosity of a carbon fiber activated with supercritical CO_2. The Journal of Physical Chemistry C, 112(13), 4991-4999.

Schutyser, W., Renders, T., Van den Bosch, S., Koelewijn, S.F., Beckham, G.T., & Sels, B.F. (2018). Chemicals from lignin: an interplay of lignocellulose fractionation, depolymerisation, and upgrading. Chemical Society Reviews, 47(3), 852–908.

Shukry, N., El-Meadawy, S. A., & Nassar, M. A. (1992). Pulping with organic acids: 3-acetic acid pulping of Bagasse. Journal of Chemical Technology & Biotechnology, 54(2), 135–143.

Sing, K.S.W. (1982). Reporting physisorption data for gas/solid systems with special reference to the determination of surface area and porosity (Provisional). Pure and Applied Chemistry, 54(11), 2201-2218.

Singh, Y., Singh, J., Sharma, S., Lam, T.-D., & Nguyen, D.-N. (2020). Fabrication and characterization of coir/carbon-fiber reinforced epoxy based hybrid composite for helmet shells and sports-good applications: Influence of fiber surface modifications on the mechanical, thermal and morphological properties. Journal of Materials Research and Technology, 9(6), 15593-15603.

Souto, F., Calado, V., & Pereira, N. (2018). Lignin-based carbon fiber: A current overview. Materials Research Express, 5(7), 072001.

Sudo, K. & Shimizu, K. (1992). A new carbon fiber from lignin. Journal of Applied Polymer Science, 44(1), 127-134.

Tachikawa, N., Park, J.W., Yoshida, K., Tamura, T., Dokko, K., & Watanabe, M. (2010). Limiting current density in ionic liquid electrolyte for lithium batteries. Electrochemistry, 78(5), 349–352.

Taira, S., Kurihara, M., Koda, K., Sugimura, K., Nishio, Y., & Uraki, Y. (2018). TEMPO-oxidized cellulose nanofiber-reinforced lignin based polyester films as a separator for electric double-layer capacitor. Cellulose, 26(1), 569–580.

Tsuchiya, H., Miyazaki, K., Iwanaga, Y., & Wakai, M. (1991). A kinetic study of cooking in solvolysis pulping with added amines. Kagaku Kogaku Ronbunshu, 17(4), 867–872.

Uraki, Y., Kubo, S., Kurakami, H., & Sano, Y. (1997). Activated carbon fibers from acetic acid lignin. Holzforschung, 51(2), 188-192.

Uraki, Y., Kubo, S., Nigo, N., Sano, Y., & Sasaya, T. (1995). Preparation of carbon fibers from organosolv lignin obtained by aqueous acetic acid pulping. Holzforschung, 49(4), 343-350.

Uraki, Y., Nakatani, A., Kubo, S., & Sano, Y. (2001). Preparation of activated carbon fibers with large specific surface area from softwood acetic acid lignin. Journal of Wood Science, 47(6), 465-469.

Vanholme, R., Demedts, B., Morreel, K., Ralph, J., & Boerjan, W. (2010). Lignin biosynthesis and structure. Plant Physiology, 153(3), 895–905.

Wang, C., Appleby, A., & Little, F.E. (2001). Electrochemical impedance study of initial lithium ion intercalation into graphite powders. Electrochimica Acta, 46(12), 1793-1813.

Wang, G., Zhang, L., & Zhang, J. (2012). A review of electrode materials for electrochemical supercapacitors. Chemical Society Reviews, 41(2), 797-828.

Westmoreland, R.A., & Jefcoat, I.A. (1991). Sulfur dioxide-ethanol-water pulping of hardwoods. Chemical Engineering Communications, 104(1-3), 101–115.

Worarutariyachai, T., & Chuangchote, S. (2020). Carbon Fibers Derived from Pure Alkali Lignin Fibers Through Electrospinning with Carbonization. BioResources, 15(2), 2412-2427.

Xu, J., Li, C.Y., Dai, L., Xu, C.L., Zhong, Y.D., Yu, F.X., & Si, C.L. (2020). Lignin-based micro-/nanomaterials and composites in biomedical applications. ChemSusChem, 13(17), 4266–4283.

You, X., Duan, J., Koda, K., Yamada, T., & Uraki, Y. (2015a). Preparation of electric double layer capacitors (EDLCs) from two types of electrospun lignin fibers. Holzforschung, 70(7), 661-671.

You, X., Koda, K, Yamada, T, & Uraki, Y. (2015b). Preparation of electrode for electric double layer capacitor from electrospun lignin fibers. Holzforschung, 69(9), 1097-1106.

Zhang, W., Yang, P., Li, X., Zhu, Z., Chen, M., & Zhou, X. (2019). Electrospun lignin-based composite nanofiber membrane as high-performance absorbent for water purification. International Journal of Biological Macromolecules, 141, 747-755.

Zheng, L., Yu, P., Zhang, Y., Wang, P., Yan, W., Guo, B., Huang, C., & Jiang, Q. (2021). Evaluating the bio-application of biomacromolecule of lignin-carbohydrate complexes (LCC) from wheat straw in bone metabolism via ROS scavenging. International Journal of Biological Macromolecule, 176, 13–25.

Acknowledgements

I would like to express my deep gratitude to Prof. Yasumitsu Uraki, my research supervisor, for his invaluable supervision, patient guidance, and tutelage during the course of my Ph.D. degree. My gratitude extends to the Japan Society for the Promotion of Science (JSPS) and Graduate School of Agriculture for the funding opportunity to undertake my studies at the Division of Environmental Resources, Hokkaido University. Additionally, I would like to express gratitude to Dr. Kengo Shigetomi for his treasured support, which was really influential in shaping my experiment methods and critiquing my results. I also thank Assoc. Prof. Keiichi Koda, Prof. Takayoshi Koike, Prof. Noboru Noguchi, and Assist. Prof. Manit Nithitanakul for their mentorship.

I would like to thank my friends, especially Apichat Trakooncheroenvit, lab mates, and colleagues for helping me with great kindness when I had problem in daily life and experiment. Great thanks also go to our department faculty, staff, and fellow students for their friendship and help. Finally, my appreciation also goes out to my family and friends in Thailand for their encouragement and support all through my studies.